Renewable Energy Storage in the Natural Gas Network: Enhancing CO_2 Conversion into Synthetic Natural Gas over Zeolite Catalysts by Tuning Ni Particle Size

Salman Amjad

Thesis to obtain the Master of Science Degree in

Energy Engineering and Management

Supervisors: Prof. José Manuel Félix Madeira Lopes

Dr. Maria Del Carmen Bacariza Rey

Examination Committee

Chairperson: Prof. Francisco Manuel Da Silva Lemos

Supervisor: Dr. Maria Del Carmen Bacariza Rey

Member of the Committee: Dr. Joaquim Miguel Badalo Branco

November 2019

Acknowledgements

First of all, I would like to express my sincere gratitude to my supervisors **Prof. Dr. José Manuel Félix Madeira Lopes** and **Dr. Maria Del Carmen Bacariza Rey** for their continuous support and motivation throughout the course of my research without whom this thesis wouldn't have seen completion.

I would also like to thank **Paula, Cátia and Auguste** and all other laboratory colleagues and friends for the good times spent and their never ending support given during this research work.

I would also like to express my humblest thanks to **KIC Inno-Energy** for their master's scholarship throughout the course of master study.

Finally, I would like to thank my family and my friends for their support, patience and understanding throughout the academic years.

Abstract

Power-to-gas constitutes a promising strategy for renewable electricity surplus storage in the natural gas network during low demand periods. In this way, developing suitable CO_2 methanation catalysts is mandatory for the application of this process under scale-up conditions. Zeolites have been reported as interesting supports for Sabatier reaction catalysts due to their tune-able properties in terms of affinity with CO_2 and H_2O. Even if in the literature mostly Ni-based zeolites have been studied, Ni^0 particles supported on monometallic zeolite catalysts typically present average sizes in the range of 20-25 nm, being required high metal loadings (10-15 wt.%) for obtaining competitive CH_4 yields.

To overcome this issue and in the context of Clean 4G project (POCI-01-0247-FEDER-038323), in this work three strategies have been followed with the final purpose of improving Ni-based catalysts dispersion over an optimized zeolite support (Cs-USY). Firstly, the incorporation of promoters such as Ce, Zr, La and Y together with Ni (co-impregnation) was studied. In a second step, the effect of the impregnation solvent used in the preparation of monometallic Ni/Cs-USY catalysts was verified, by comparing water, ethanol, methanol, 2-propanol, acetone and ethylene glycol. Finally, the application of a new synthesis method of nickel nanoparticles, sol-gel, was explored. All catalysts were applied in CO_2 methanation reaction and characterized using TGA, XRD and H_2-TPR. Yttrium was found as the most favourable promoter, 2-propanol as the best solvent and sol-gel technique did not favour the performances due to the larger Ni particle sizes formed (50 nm).

Keywords: CO_2 methanation, zeolite-supported catalysts, promoters, impregnation solvent, sol-gel method.

Resumo

O armazenamento da energia renovável produzida em excesso pontualmente na rede de gás natural (*Power-to-Gas*), representa uma estratégia promissora para aumentar a competitividade do uso de fontes não fósseis, diminuindo as emissões de CO_2. Neste sentido, é prioritário desenvolver catalisadores eficientes para o processo de metanação do CO_2 possibilitando a sua implementação a nível industrial. O uso de catalisadores de Ni suportados em zeólitos para esta reação foi identificado como favorável, uma vez que permite a otimização das suas propriedades em termos de afinidade com o CO_2 e a H_2O. Habitualmente, as partículas de Ni^0 suportadas em zeólitos apresentam tamanhos na gama dos 20-25 nm, implicando o uso de teores elevados de metal para que se obtenham rendimentos de metanação competitivos.

O presente trabalho, desenvolvido no contexto do projeto *Clean4G* (POCI-01-0247-FEDER-038323), teve como objetivo obter partículas de Ni mais pequenas e melhorar a sua dispersão em catalisadores à base de zeólitos. Assim sendo, foram estudados o efeito da incorporação de promotores por co-impregnação (Ce, Zr, La e Y), a utilização de diferentes solventes durante a impregnação (água, etanol, metanol, 2-propanol, acetona e etileno glicol), e a síntese e posterior incorporação de nanopartículas de Ni pelo método sol-gel. As amostras foram testadas em condições de metanação e caracterizadas por TGA, XRD e H_2-TPR. O ítrio foi identificado como o melhor promotor e o 2-propanol o melhor solvente. Pelo contrário, o método sol-gel não aumentou o rendimento do processo uma vez que as partículas de Ni formadas apresentaram tamanhos de ~50 nm.

Palavras chave: Metanação do CO_2, catalisadores suportados em zeólitos, promotores, solvente da impregnação, método sol-gel.

Table of contents

List of figures

List of tables

Nomenclature

GHG: Greenhouse Gases

EES: Electric energy storage

SNG: Synthetic natural gas

CNG: Compressed natural gas

RWGS: Reverse water gas shift reaction

EFAL: Extraframework aluminum species

FTS: Fischer- Tropsch synthesis

DRM: Dry reforming of Methane

TGA: Thermogravimetric analysis

XRD: X-ray Diffraction

TPR: Temperature programmed reduction

TMA: Tetramethylammonium

1. Introduction

Climate change is one of the most important worldwide environmental issues nowadays. In addition, renewable energy sources have been extensively used to help in climate issues but their intermittency can compromise grid stability. Consequently, it is necessary to develop suitable energy storage systems which could store excess renewable energy, promoting its application in large scales and, thus, fighting climate change. In this way, power-to-gas has been reported as a promising alternative since, by this strategy, the surplus electricity can be stored in the natural gas network as synthetic natural gas.

Power-to-gas alternative is based on the use of surplus electricity for the production of renewable hydrogen. This H_2 will be later used for reducing CO_2 into CH_4 (CO_2 methanation). The activation of the carbon dioxide requires the use of catalysts. Indeed, several noble metals (Rh, Ru, Pd) and VIIIB group elements (especially Ni) based on different supports such as Al_2O_3, SiO_2, Ce/Zr mixed oxides, mesoporous materials, carbon, hydrotalcite-derived materials or even zeolites have been studied and reported in the literature.

Among all, Ni-based zeolites gained attention in recent times due to their tunable properties. Indeed, parameters such as the zeolite type, the structure composition or even the metal loadings have been focus of study in the literature. Even if optimized zeolite-based materials with higher performances that commercial hydrogenation catalysts have been reported, the main drawback of these systems remains in the sintering of Ni species leading to Ni^0 particles in the range of 20-25 nm. Consequently, further efforts must be done for overcoming this issue.

Thus, the objective of the present work was to obtain Ni-based zeolite catalysts with smaller particles than those reported in the literature. For this purpose, three strategies were studied by fixing the Ni loading (15 wt.%) and the zeolite support (Cs-USY) in accordance with previous studies carried out in the research group. Firstly, the incorporation of promoters by co-impregnation was carried out, using Ce, Zr, La and Y. Secondly, the nature of the impregnation solvent used in the preparation of 15Ni/Cs-USY samples was tuned, using water, ethanol, methanol, 2-propanol, acetone and ethylene glycol. Finally, a new preparation method was studied (sol-gel) in order to synthesize Ni nanoparticles to be later incorporated by three methods (co-calcination, mechanical mixture and impregnation) to the Cs-USY zeolite support. All samples were characterized by thermogravimetric analysis (TGA), X-ray diffraction (XRD) and temperature programmed reduction with hydrogen (H_2-TPR). Finally, materials

were tested in CO_2 methanation reaction, using a H_2/CO_2 ratio of 4 and temperatures ranging from 250 to 450 °C.

In the present work, a literature review of the topic can be found in Chapter 2. In addition, catalysts preparation procedures and conditions as well as information regarding the characterization techniques used and the catalytic test unit are presented in Chapter 3. Furthermore, characterization and catalytic tests results obtained are exposed in Chapter 4. Finally, the most important conclusions and some perspectives for future studies are shown in Chapter 5.

The present Master Thesis was developed in the context of Clean 4G project (POCI-01-0247-FEDER-038323, partners: Secil S.A., GSYF Clean Energies, CERENA/IST and CQE/IST). More specifically, this work contributed to this project in the task of developing of CO_2 emissions from cement industry to synthetic natural gas using renewable hydrogen (carbon dioxide methanation reaction).

2. Literature review

2.1. Motivation

2.1.1 Climate variability and need for energy storage

In Paris, 2015, UN climate change conference, 175 countries signed the agreement on limiting the rise in temperature to 2 ^{0}C due to global warming. Such an aim requires strong efforts and especially reduction in the human activities which cause the global greenhouse gas emissions (GHG). Keeping this view in mind, many countries across the globe have already started their efforts and still trying to change their energy mix [1].

As shown in Figure 1, share of the renewable energy in gross final energy consumption was 17.5% across EU 28 in 2017 as compared to 8.5% in year 2004. Also EU intends to have 20% shares of renewable energy sources in its final gross energy consumption by 2020.

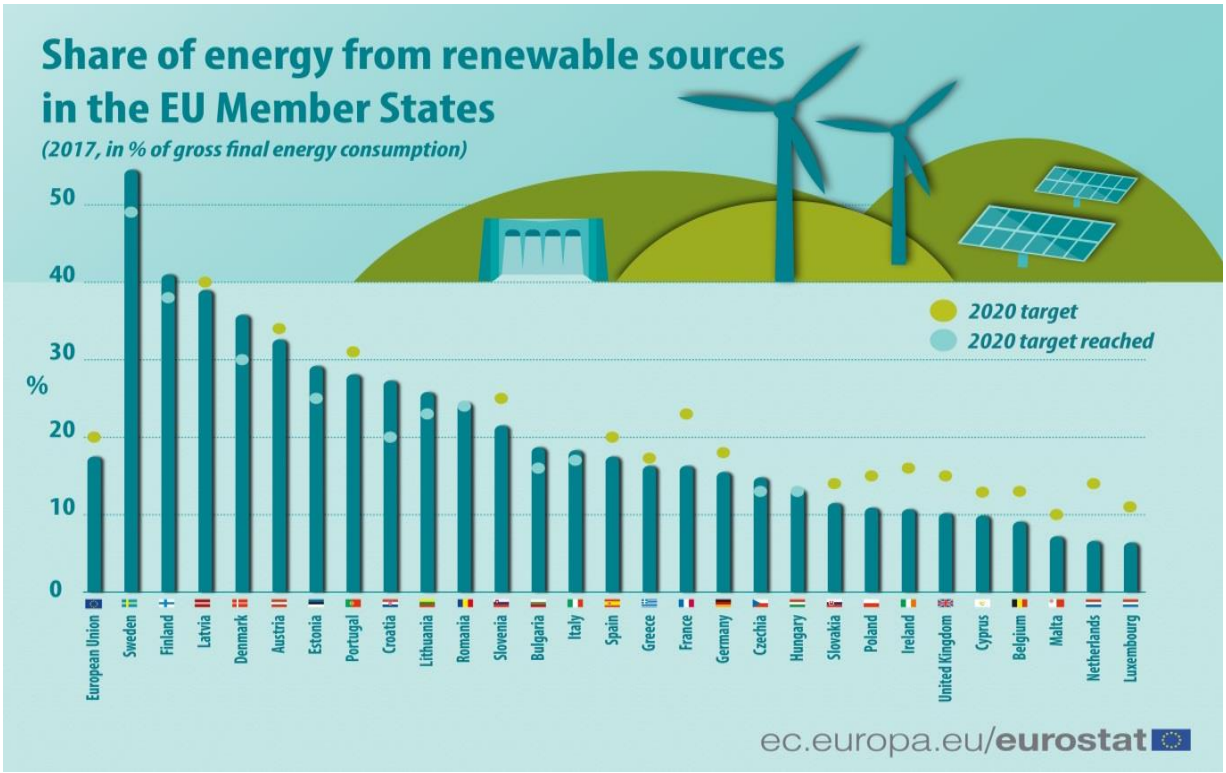

Figure 1: Share of renewable energy source in final energy consumption, 2017, source: Eurostat.

By 2050, the EU climate foundation has the objective to achieve 100% renewable share in their energy mix [1]. As these renewable energy sources have potential to balance the energy demands, this objective seems to be at least physically realistic [2].

However, as renewable energy sources such as wind and solar are intermittent, their increase share in energy supply systems put questions on their steadiness and reliability for energy production. Since already existing electrical power networks rely on constant energy flow, intermittent generation from renewable energy sources demands flexibility within the system. In this way, there is an increased interest for electric energy storage (EES) systems, which could provide a suitable solution for uneven supply and demand whenever there are intermittency issues or surplus renewable energy [3]. Consequently, a definitive extension of renewable energy systems will be allowed.

2.1.2 Electrical energy storage (EES) systems

Electrical energy storage technologies can be classified by form of storage, as shown in Table 1. Among all, chemical energy storage has gained much attention in recent years.

Table 1: Types of EES systems by form of storage [4].

Form of storage	Type of energy	Examples
Electrical	Electrostatic	Capacitors, super capacitors
	Magnetic/current	Superconducting magnetic energy storage (SMES)
Mechanical	Kinetic	Flywheels
	Potential	Pumped hydroelectric storage (PHS), compressed air energy storage (CAES)
Chemical	Electrochemical	Conventional batteries (lead-acid, Ni hydride, Li ion), flow-cell batteries (Zn bromine and V redox)
	Chemical	Fuel cells, molten-carbonate fuel cells (MCFCs), metal-Air batteries
	Thermochemical	Hydrogen, metals, ammonia, methane
Thermal	Low temperature	Aquifers cold energy storage, cryogenic energy storage
	High temperature	Sensible heat systems (steam, hot water accumulators, graphite, hot rocks and concrete), latent heat systems (phase change materials)

An example of chemical energy storage is described in Figure 2 where scattered sunlight is concentrated by using a parabolic mirror and used to drive an endothermic reaction and produce chemical fuels which can be stored, transported and used when needed [4]. Another possibility,

deeply discussed later in this work, is to use renewable energy surplus to carry out water electrolysis so that renewable energy can be stored as H_2 (power-to-gas).

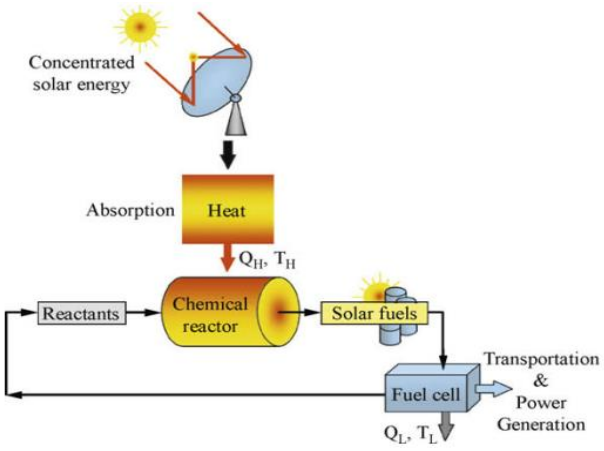

Figure 2: Conversion of solar energy into solar fuel [4].

2.2. CO_2 Conversion into fuels: a potential alternative for renewable energy storage

CO_2 conversion has been widely reported as a promising route for the reduction of greenhouse gases emissions. Indeed, there are various different possible options to carry out the CO_2 transformation into valuable products (see Figure 3) but in all cases there is still margin for improvement in terms of technology and catalyst design to get optimized results in the overall performance of the process [5].

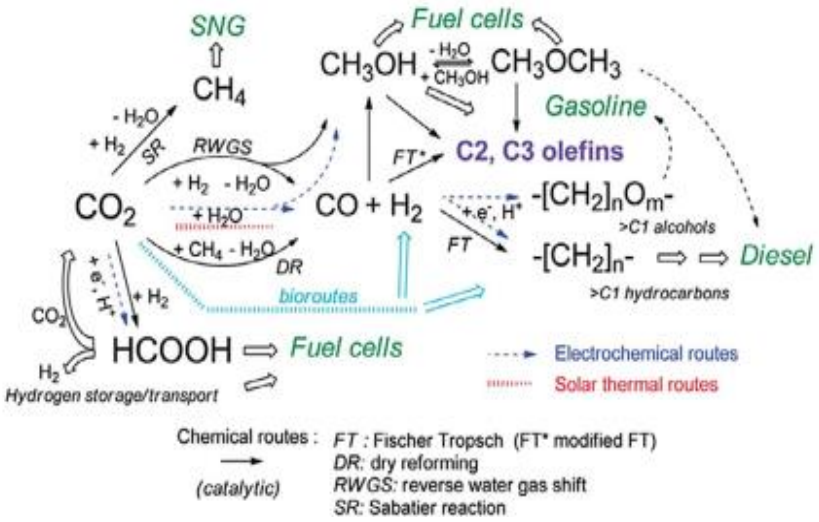

Figure 3: Possible routes to produce chemical fuels using synthesis gas [5].

Among all the alternatives, CO_2 hydrogenation is the most reported pathway for carrying out CO_2 transformation into valuable products such as CH_4, CH_3OH and C_2H_6. However, it is certain that CO_2

conversion through this mentioned route will be feasible only if produced by using renewable hydrogen [6]. As previously pointed out, the application of power-to-fuel approach allows the production of renewable hydrogen from surplus wind and/or solar energy through water electrolysis. Consequently, the utilisation of CO_2 as source of carbon for the production of fuels by incorporating excess renewable energy constitutes a promising way for limiting greenhouse gases emissions as well as effectively dealing with the intermittency of renewable energy sources, as it helps to store surplus renewable energy into chemical fuels through "power-to-fuel" concept.

2.3. Power to methane

2.3.1 Potential as energy storage alternative

As already referred, the application of power-to-gas approach for CO_2 valorisation into synthetic natural gas (SNG) has potential to play a remarkable role in tackling the issues of long term as well as large capacity renewable energy storage. Indeed, a comparison of different storage technologies in relation with storage capacity vs. charge/discharge timing is depicted in the Figure 4. As seen, only chemicals based fuels (SNG) can fulfill the requirement for the long term and long capacity energy storage. Contrary to this, other storage technologies such as batteries and flywheel are limited and thus can supply stored energy for short term fluctuations only [7][8].

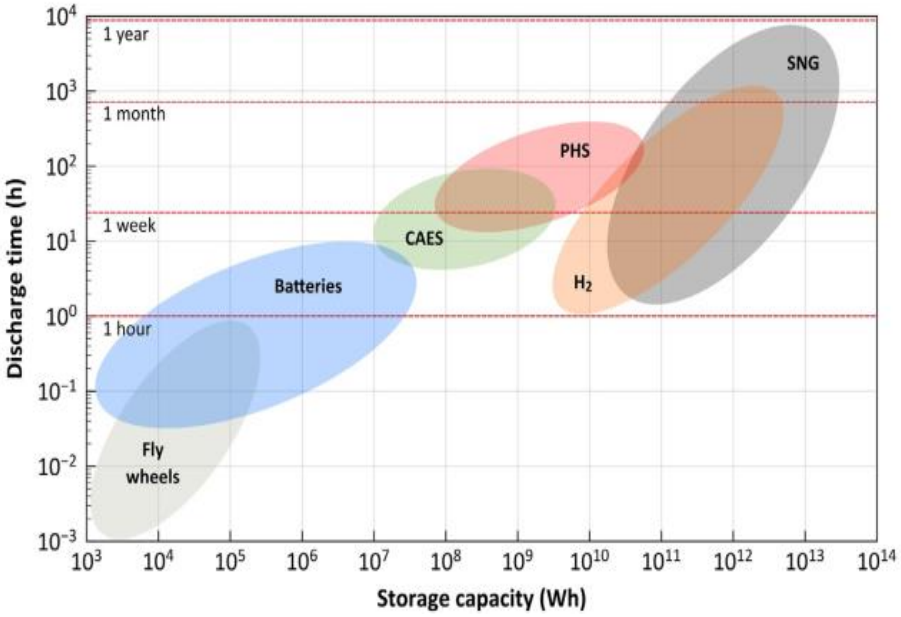

Figure 4: Storage capacity and discharge time for several energy storage technologies [7].

To summarize the P2G concept, this is a three step process generation of electrical energy by use of renewable energy sources, use of excess renewable electrical energy to produce renewable hydrogen

(H_2) by water electrolysis, and lastly use of renewable hydrogen into thermochemical conversion of CO_2 to methane gas (CH_4) via the Sabatier reaction [8]. This renewable CH_4 then can be introduced into natural gas network grid or even used in transportation (CNG cars), heating applications and in gas fired power plants, as presented in Figure 5.

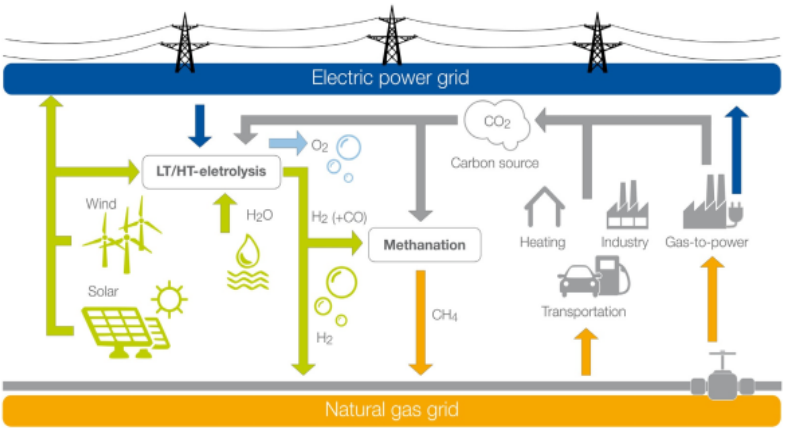

Figure 5: Power-to-gas concept incorporating surplus renewable energy as well as utilization of carbon source as carbon neutral-cycle [8].

2.3.2 CO_2 methanation: The Sabatier reaction

Brodie, in 1872, first described the reduction of carbon oxides into methane with the application of electric discharge. Then, after thirty years, Jean-Baptiste Senderens and Paul Sabatier discovered the same hydrogenation catalysts with applied knowledge of heterogeneous catalysis. Furthermore, in 1912, Noble prize was awarded to Sabatier for his work "method of hydrogenating organic compounds in the presence of finely disintegrated metals" [8].

$$\boldsymbol{CO_{2\,(g)} + 4H_{2(g)} \rightarrow CH_{4(g)} + 2H_2O_{(v)}} \qquad \textbf{(1)}$$

In carbon dioxide methanation reaction process (Equation (1)) H_2 and CO_2 are converted into the CH_4 and H_2O. The high chemical stability of CO_2 requires the use of a catalyst for its activation and conversion. CO_2 methanation has been reported by electro-, photo-, plasma and thermal processes [9][10][11]. Among the different approaches, the conventional thermal catalysis route has been the most deeply analysed in the literature [12][13][14].

2.3.3 Thermodynamics

CO_2 methanation is a reaction sensitive to temperature, pressure and reactants composition. Indeed, Gao *et al.* [15] reported that the theoretical operating temperature window for CO_2 conversion into methane is <500 °C due to overall exothermic nature of the reaction. At higher temperatures

(>500°C) reverse water gas shift reaction (RWGS) dominates, therefore most of the methanation studies are below temperature <500°C. High reaction temperatures could increase the reaction rate but this will also demand higher catalysts stability and could cause carbon deposition. Additionally, high pressures (1-100 atm) were found to favor methanation reaction as this reaction is accompanied with a decrease in the number of moles. However, a pressure range of 10-30 atm is considered optimal in terms of catalysts stability and sintering issues. Moreover, if H_2/CO_2 ratio is greater or equal to the stoichiometry then sintering as well as carbon deposits is not favoured. Finally, author also studied the effect of adding steam to the reactor feed and found out no effect on methane selectivity but a decrease in CO_2 conversion, together with carbon deposition. To sum up, methane yield > 99% can be obtained from the above discussed conditions (i.e. T <500 °C, pressures till 30 atm and H_2/CO_2 ratio of 4).

2.3.4 Catalysts

CO_2 methanation has been focus of hundreds of research in the last years, being verified that the efficiency of the CO_2 methanation reaction depends on the catalyst used. Different metal supported catalytic systems have been reported in the literature. Among all, the most commonly used active sites were Group VIIIB metals, Rh [16], Ru [17], Pd [18]) and Ni [19] and the main supports Al_2O_3, SiO_2, TiO_2, Ce–Zr mixed oxides [19][20][21][22]. Among all, Ni supported catalysts have been the most commonly used and studied for this reaction due to their higher activity and abundant supply for lower cost. However, Ni-based catalysts are prone to sintering, which causes decrease in metallic dispersion and can be also responsible for deactivation at low temperatures, probably due to the formation of mobile nickel sub-carbonyls by the interaction with CO [14].

Regarding the supports, zeolites have been also reported as promising supports for methanation reaction due to its easily tunable properties [23][24]. Several parameters such as their potential basic properties, the high affinity to CO_2, the hydrophobic character or the hydrothermal stability (in the case of USY zeolite) were found as favorable for obtaining active, selective and stable optimized zeolite catalysts for CO_2 methanation [25][26][27][28][29][30][31][32][33]. Indeed, monometallic Ni samples based on zeolite supports presented good performances, irrespective of their relatively large particle sizes (20-25 nm) and the main location of the metal particles on the outer surface, probably due to the enhanced metal-support interactions established [19]. Generally, it is known that small Ni particles and strong metal-support interactions could suppress deactivation and sintering processes, enhancing the catalytic performances. Keeping this view, the modification of Ni-Zeolite catalysts

through the incorporation of the promoters or the modification of the preparation procedures could be a promising research topic for enhancing the performances of these materials [34].

2.4. Zeolite-based catalysts for CO_2 methanation reaction

As already referred, zeolites have been reported as suitable supports for CO_2 methanation reaction [25][26][27][28][29][30][31][32][33]. In line of this, the main findings reported in the literature for this type of materials applied in CO_2 methanation are summarized below:

↑ **Metallic Phase dispersion:** Preparation conditions (calcination and reduction temperatures, preparation method) are known to affect metal phase dispersion. Indeed, higher calcination temperature leads to a reduction in metal reducibility and sintering issues. Additionally, with the increase of pre-reduction temperature reducibility increases with decrease in metal dispersion probably due to metal sintering at higher temperatures which demands incorporation of promoters such as Ce [31], Mg [32], La [35]. Moreover, research results also verified that impregnation leads to be best catalytic performance when compared to ion exchange [19].

↑ **Basicity and affinity towards CO_2:** Si/Al ratio and cation size play an important role in achieving higher basicity and provide additional CO_2 adsorption and activation sites. Indeed, zeolite exchanged with larger cations such as Cs^+ and K^+ rather than Li^+ or Na^+ presented higher affinity towards CO_2. Additionally, low Si/Al ratio zeolites present more exchange positions, proving a great number of carbon dioxide adsorption sites.

↑ **Hydrophobicity:** H_2O is a reaction product and, in the case of zeolites, it competes with CO_2 for the same adsorption sites. The interaction/affinity between water and zeolites can be changed by tuning with Si/Al ratio. Indeed, higher Si/Al ratios lead to more hydrophobic surfaces reducing the inhibitory role of water in the reaction.

↑ **Resistivity towards steam:** Water produced during the methanation reaction may destroy zeolites structure. To cope up with this issue, the use of ultrastable Y zeolites (USY) presents advantages, since these materials are known to be hydrothermally stable.

In terms of the carbon dioxide mechanism over zeolites, Westermann *et al.* [36] proposed an approach for over Ni/USY zeolites prepared by impregnation. In absence of hydrogen, CO_2 was suggested to be adsorbed on extraframework Al species (EFAL species) and/or exchangeable cations (e.g. Na^+), being further converted into formates by the H atoms dissociated in Ni^0 sites. Till 300 ^{0}C, almost all of these formates were dissociated to carbonyls because CH_4 formation was quite low.

Above 350 ^{0}C these carbonyl and formyl species got further hydrogenated on Ni^{0} particles to produce formaldehydes, methoxy species and, lastly, methane, as seen in Figure 6.

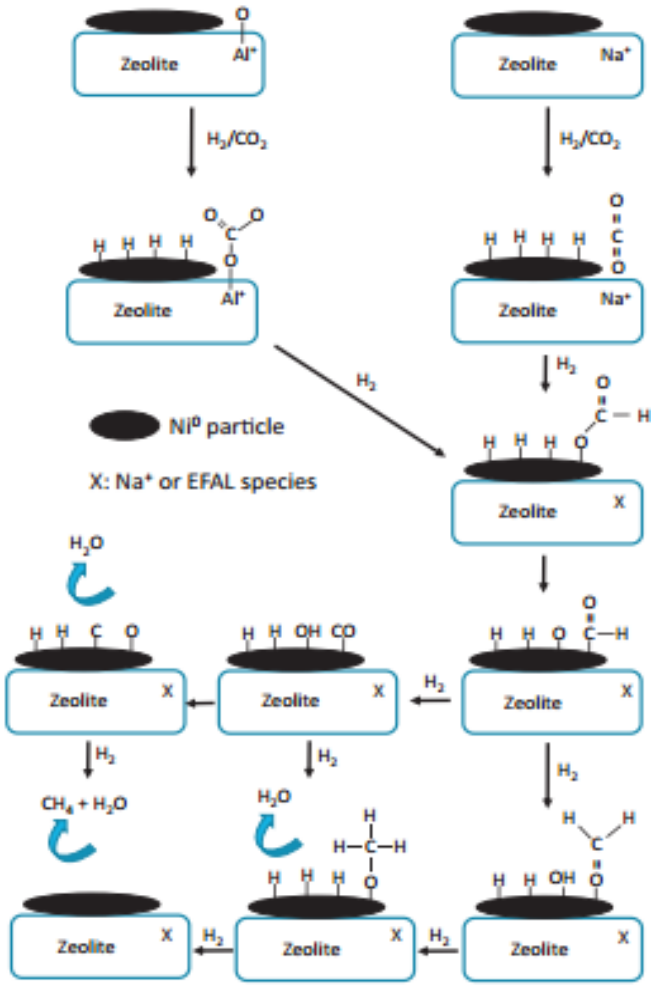

Figure 6: Proposed methanation mechanism over Ni/USY zeolites [37].

2.5. Strategies for improving metallic dispersion in Ni-based catalysts

As already referred, Ni is the main active metal incorporated on carbon dioxide methanation catalysts but its main problem is related to the severity of sintering processes. To avoid deactivation, several strategies related with the preparation or even composition of materials can be carried out such as incorporating promoters (Ce [27][33], La [35], Mg [37][38][39][32], Fe [40], Cu [41], and Pt [42]) tuning the preparation conditions (calcination and pre-reduction temperature [26], impregnation solvent [37][38][39][32], preparation method [19][33]) or even trying new methods (sol-gel [43][44][45], one-pot HS [46], grafting [47]). Among all the possible strategies, three of them will be deeply described below:

2.5.1 Promoters incorporation

As already referred, one of the strategies to improve metallic phase dispersion in supported Ni based catalysts is to incorporate promoters. Several promoters have been studied in literature (e.g. transition metals, noble metals, lanthanides, group alkali earth metals) and some of these studies are summarized below.

To start, Trovarelli *et al.* [48] prepared Rh/SiO_2 catalysts promoted with CeO_2 and compared them with un-promoted Rh/SiO_2 and Rh/CeO_2 samples. Authors verified that the activity of the original catalysts was greatly enhanced by the addition of CeO_2 as promoter. Authors attributed this beneficial effect of Ce addition to the surface vacancies created at the interface between Rh and reduced CeO_2, enhancing CO_2 activation. Moreover, they also concluded that the presence of Rh causes an increase in the re-dispersion of CeO_2 crystals. Additionally, similar positive effects of CeO_2 addition were reported by Rahmani *et al.* [49] for Ni based catalysts supported on mesoporous material γ-Al_2O_3.

Furthermore, Ahmad *et al.* [50] synthesized a series of Ni catalysts supported on γ-Al_2O_3 (5%X-12%Ni/γ-Al_2O_3 (X= La, Ce, Pr, Eu and Gd) to evaluate the effect of lanthanides on methanation reaction activity as well as Ni dispersion. They verified that 5%Pr-12%Ni/γ-Al_2O_3 catalyst showed the best results with highest CO_2 conversion (98.2 %) and CH_4 selectivity (100%) under reaction reactions. Also, higher Ni dispersions without remarkable effects on textural properties were observed for lanthanides promoted catalysts when compared to 12%Ni/γ-Al_2O_3 reference material.

In addition, Park *et al.* [38] prepared highly dispersed Pd–Mg/SiO_2 catalysts using reverse micro-emulsion method for CO_2 methanation. Indeed, authors found out that Pd particles size were reduced to the range of 5 to 10 nm. Moreover, at 450 ^{0}C, CO_2 conversion of 59% and CH_4 selectivity of 95% were observed, being these values higher than those obtained for un-promoted Pd/SiO_2 catalysts, being the beneficial effect of Mg incorporation attributed to the occurrence of synergistic effects between Pd and Mg species. Moreover, replacing Mg by Fe or Ni led to higher activity for CO_2 conversion but Fe-containing catalyst resulted into low selectivity for methane.

Also, Boix *et al.* [42] prepared Pt-Co mordenite with different loadings of both metals verifying that bimetallic samples presented better performances in terms of activity in comparison monometallic catalysts, with the best Co/Pt ratio being 0.6. The promoting effect of Pt was attributed to the increase in hydrogen activation and the formation of intermediate active species $PtCo_xO_y$.

2.5.2 Variation of the impregnation solvent

Catalysts preparation conditions are key parameters as during this process every single step might influence the properties of the final materials and, thus, their catalytic performances. According to the literature, the nature of the impregnation solvent can positively affect the metal-support interactions [51][52][53][54][55][56][57]. In this way, a summary of some works dealing with this topic is presented below.

Firstly, Qiu *et al.* [53] prepared Ni nanoparticles over SBA-15 by co-impregnation using ethylene glycol (EG) for reforming reaction of methane and they found out that EG addition with the metal nitrate aqueous salt solution promotes Ni species migration towards confined channels of the SBA-15 support used. Moreover, Ni/SBA-15 catalyst impregnated with Ethylene glycol (EG) demonstrated resistance to sintering and proved to be thermal stable in dry reforming of methane. They suggested that the reason for this beneficial effect was the decrease of the impregnation solution surface tension when using EG, what favoured the diffusion into the mesoporous channels of the SBA-15 material. Moreover, similar positive enhancements were observed when Trisunaryanti *et al.* [54] synthesized catalysts with well dispersed Ni nanoparticles supported on SBA-15 for cellulose hydrocracking reaction using co-impregnation of EG together with the metal salt solution. Indeed, authors verified an homogenous distribution of Ni nanoparticles in the catalyst without nickel aggregates when using this improved impregnation method.

Also, Lucredio *et al.* [55] studied the effect of the impregnation solvent in the preparation of catalysts for application in the steam reforming of ethanol. Indeed, they prepared 10 wt. % Co catalysts supported on SiO_2 using methanol and water as impregnation solvents and verified that methanol led to smaller Co particles when comparing to the simple aqueous solution. Consequently, the sample prepared using methanol showed the best catalytic performances.

Furthermore, Zhang *et al.* [56] prepared Co catalysts supported on silica for Fischer Tropsch synthesis (FTS) reaction using different solvents to check the effects on the properties of the silica support, metal dispersion and species reducibility. The use of ethanol led to the smallest cobalt particles and the highest metallic dispersion. As the activity of these catalysts during the reaction only depended on the number of active sites on the surface of the reduced metal which is determined by the Co particle size and reduction degree, ethanol sample presented the highest conversion.

Finally, Ho and Su [57] studied the effect of ethanol as impregnation solvent for Co supported on SiO_2. They found that ethanol presented a positive effect due to the increased interaction between

Co and SiO_2, which resulted in the decrease in crystal size of cobalt species. Indeed, Song and Ozkan [58] found the same effect in the dispersion of Co particles over CeO_2 catalysts for steam reforming reaction when using ethanol as solvent.

2.5.3 New preparation methods: Sol-Gel

Finally, other strategy which could eventually lead to smaller Ni particles is to tune the preparation method. Indeed, several works (some of them summarized below) used sol-gel approaches for obtaining well dispersed metal nanoparticles for catalytic applications. In this way, Branco *et al.* [43] studied Ni-based bimetallic catalysts prepared by sol-gel method for partial oxidation of methane. They found that the synthesized materials were active and selective for the studied application as methane conversion was 50-70 % and syngas selectivity to H_2 and CO were 60-90 % and 50–80 %, respectively, even at relatively low reaction temperatures (550-650 ^{0}C). Moreover, this prepared catalysts also showed long term stability and low carbon deposition when compared to other Ni based materials reported for the same reaction.

Also, Danial *et al.* [44] performed experiments with NiO nanoparticles prepared by sol-gel in electrocatalytic oxidation of glucose. They verified that the performances were significantly enhanced by this preparation method, even at less favorable reaction conditions.

Furthermore, Aghamohammadi e*t al.* [45] studied the effect of the synthesis method in preparing Ni/Al_2O_3-CeO_2 catalysts for dry reforming of methane (DRM). When comparing to impregnated samples, they observed that sol-gel samples presented smaller particle sizes and higher metallic phase dispersion on the support. Moreover, sol-gel samples resulted in higher conversions and yield (higher H_2/CO molar ratio) at different operating conditions.

Then, Rodemerck *et al*. [59] prepared Ni/SiO_2 catalysts using sol-gel as an attempt to reduce Ni particles size for steam reforming of methane. They found that sol-gel (polymer-assisted synthesis) produced Ni nanoparticles of very small size (8-11 nm), which resulted in high dispersion as well as high metal-support interactions. Moreover, catalysts prepared with sol-gel showed higher activity and stability towards the studied reaction.

Finally, Ali *et al.* [60] studied the performances of 5 wt.% Ni nanoparticles supported on Silica-Alumina materials prepared using sol-gel technique for methane reforming. The resulted Ni nanoparticles exhibited exceptional performances in terms of catalyst activity and stability when comparing to samples prepared by conventional impregnation method. These results were attributed

to the higher metallic dispersion, higher reducibility and small metal particle sizes (6 nm) in the sol-gel material.

To conclude, Pechini modified sol-gel method (which involves the combination of metal salts with ethylene glycol and citric acid to form homogenous metal/citrate complexes followed with a thermal treatment [61]) could constitute a simple and low-cost method for testing the potential of sol-gel in the preparation of Ni-based catalysts.

2.6. Objective

As seen in the present chapter, developing active, selective and stable catalysts towards carbon dioxide methanation constitutes an important focus of research nowadays. Indeed, and being zeolites promising supports for this reaction but with limitations in terms of Ni particles average sizes (typically 20-25 nm in absence of promoters), it is crucial to further explore the potential of these materials for CO_2 methanation with special focus in obtaining well dispersed metallic phase. For this purpose, three strategies will be followed by using as support a material optimized in previous studies (Cs-USY):

- **Incorporation of promoters**: the addition of both new and well-known promoters will be carried out by an optimized preparation method (co-impregnation) and fixing the Ni loading as 15 wt.% and the promoter loading also as 15 wt.%;
- **Change in the impregnation solvent**: equivalent preparations of 15 wt.% Ni samples will be carried out by using as impregnation solvent water, ethanol, methanol, 2-propanol, acetone and ethylene glycol;
- **Evaluation of new preparation methods**: Pechini-modified sol-gel method will be tested for preparing 15 wt.% Ni-containing catalysts. Three strategies will be followed after the synthesis of the nickel nanoparticles: co-calcination in presence of the used zeolite, mechanical mixture and impregnation.

3. Experimental Work

3.1. Strategy

As previously discussed, the purpose of this work is the application of different approaches for obtaining highly dispersed Ni particles over Ni/Zeolite catalysts for CO_2 methanation reaction. Consequently, three pathways schematically presented in Figure 7 and properly discussed in the next pages were followed.

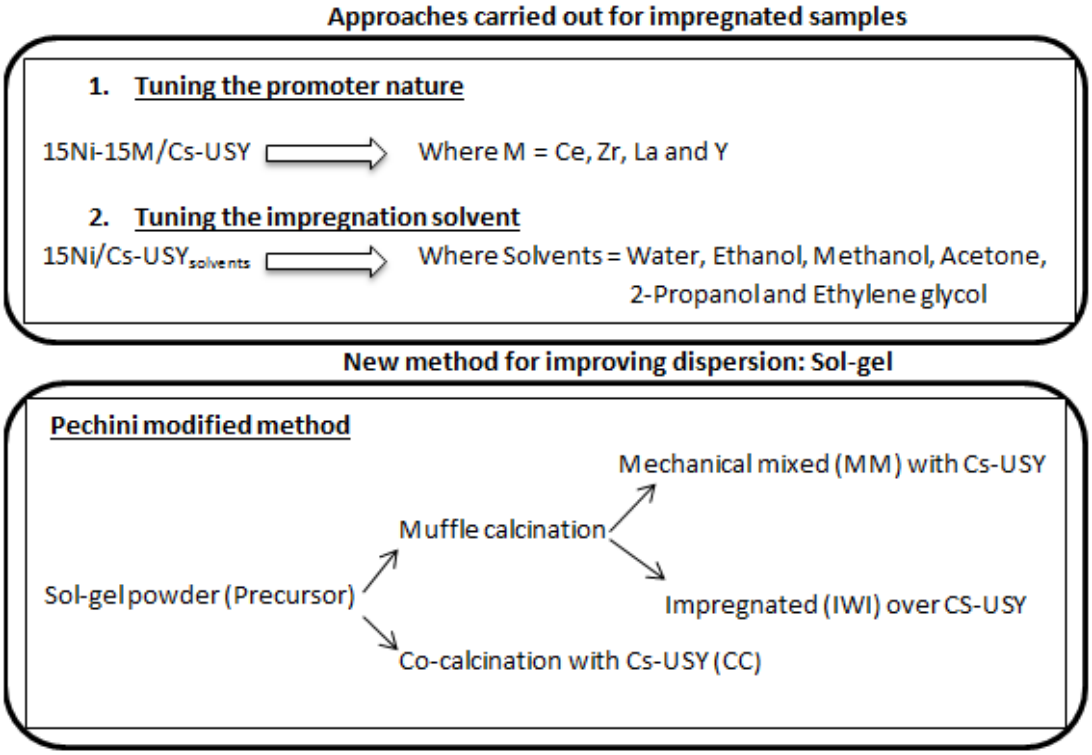

Figure 7: Strategies followed for tuning Ni particle size.

3.2. Catalysts preparation

As a first step, an optimized zeolite support was prepared by taking into account previous studies carried out in this research group [25][26][27][28][29][30][31][32]. Consequently, a commercial USY zeolite supplied by Zeolyst containing a global Si/Al ratio of 38 was modified in order to obtain the Cs-USY form chosen as support for this work. The preparation was carried out by using a certain mass of commercial USY zeolite (12 g) and mixing it with a 1 M $CsNO_3$ solution keeping a $V_{solution}/m_{zeolite}$ = 4 ml g^{-1}. The suspension was continuously stirred for 4 h at room temperature and then filtered under vacuum with distillated water until neutral pH = 7 was achieved. Finally the sample was dried in oven

overnight at 100 ^{0}C. This procedure was repeated three times and then calcination was carried out at 500 ^{0}C under air flow (60 ml min^{-1} g^{-1}) for 6 h using a heating rate of 2 ^{0}C/min (Figure 8).

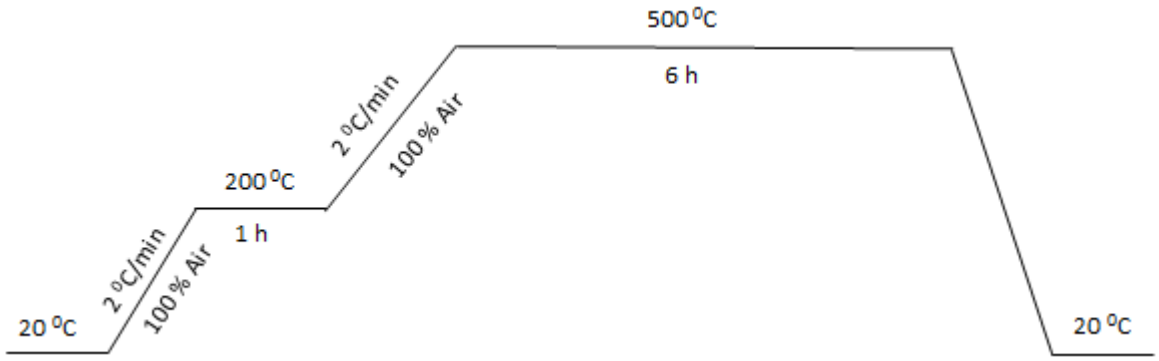

Figure 8: Temperature profile for calcination.

3.2.1 Promoter nature effect over 15%Ni-15%M/Cs-USY catalysts

In this first approach, the effect of adding different promoters (M = Ce, Zr, La, Y) over Ni-based Cs-USY catalysts was evaluated. Samples were prepared by co-impregnating 15 wt.% Ni and 15 wt.% promoter over the support support [33]. Indeed, Ni and promoters precursor salts were used for preparing an aqueous impregnation solution incorporated to the support in a drop wise manner under continuous stirring. Samples were then dried overnight at 80 ^{0}C and calcined using the conditions presented in Figure 8. Their main characteristics are summarized in Table 2.

Table 2: Preparation conditions and codes of the samples prepared for the promoter nature (M) study.

Label	wt. % Ni	wt. % M	Preparation method	Impregnation solvent	$T_{calcination}$ ($^\circ$C)
15%Ni-15%Ce/Cs-USY	15	15	Co-impregnation	Water	500
15%Ni-15%Zr/Cs-USY					
15%Ni-15%La/Cs-USY					
15%Ni-15%Y/Cs-USY					

3.2.2 Impregnation solvent effect over 15%Ni/Cs-USY catalysts

In this second approach, the effect of the impregnation solvent nature (water, ethanol, methanol, 2-propanol, acetone or ethylene glycol) in the characteristics and performances of Ni/Cs-USY catalysts containing 15 wt. % of Ni incorporated by incipient wetness impregnation was studied. For incipient wetness impregnation, a solution of $Ni(NO_3)_2{\cdot}6H_2O$ (Sigma Aldrich, >99%) prepared by using a solvent volume close to the zeolite pores was added drop wise to the Cs-USY support under

continuous stirring. After this, drying in oven at 80 ^{0}C and calcination (Figure 8) were carried out. Table 3 presents the main characteristics of the catalysts from this chapter.

Table 3: Preparation conditions and codes of the samples prepared for the impregnation solvent study.

Label	wt. % Ni	Preparation method	Impregnation solvent	$T_{calcination}$ (°C)
15% Ni/Cs-USY$_{Water}$	15	Incipient wetness impregnation	Water	500
15% Ni/Cs-USY$_{Ethanol}$			Ethanol	
15% Ni/Cs-USY$_{Methanol}$			Methanol	
15% Ni/Cs-USY$_{2\text{-}Propanol}$			2-Propanol	
15% Ni/Cs-USY$_{Acetone}$			Acetone	
15% Ni/Cs-USY$_{Ethylene\ glycol}$			Ethylene glycol	

3.2.3 Preparation method: Sol-gel

In this last study, one of the methods commonly applied for preparing nanoparticles (sol-gel) was explored. In this way, NiO nanoparticles were prepared by Pechini modified method [61][43][59][60]. For this, Ni nitrate Ni $(NO_3)_2.6H_2O$ salt was mixed with citric acid (1:3) and then ethylene glycol was added (2:3 mol/mol of ethylene glycol and citric acid, respectively). The solution was kept at ~80 ^{0}C under mechanical stirring for about 4 h till the formation of a gel (after the removal of water through evaporation). Then, the obtained gel was dried in oven at 200 ^{0}C for 24 h. At this point and as also shown in Figure 7, two approaches were followed. On one side, a specific mass of NiO nanoparticles precursor powder for obtaining a final loading of 15 wt. % Ni (determined by performing a TGA-DSC analysis of the precursor powder) was calcined in presence of the corresponding mass of Cs-USY zeolite under air flow using conditions presented in Figure 8. This process was named as co-calcination (CC). On the other side, the NiO nanoparticles precursor powder was calcined in muffle at 500 °C for 6 h and then the resulting NiO nanoparticles were mechanical mixed (MM) and impregnated (IWI, using a TMAOH 1 M solution) over the corresponding Cs-USY mass in order to obtain 15 wt.% Ni catalysts. The main characteristics of these samples are summarized in Table 4.

Table 4: Preparation conditions and codes of the samples prepared for sol-gel method study.

Label	wt. % Ni	Preparation conditions	$T_{calcination}$ (°C)
NiO $_{SG}$	100	Sol-gel and calcination in muffle	500
CC [15% NiO $_{SG}$ - Cs-USY]	15	Co-calcination of NiO $_{SG}$ precursor powder in presence of Cs-USY under air flow	
MM [15% NiO $_{SG}$ + Cs-USY]		Mechanical mixture of NiO $_{SG}$ with Cs-USY	

IWI [15% NiO_{SG}/Cs-USY]	Incipient wetness impregnation of NiO_{SG} over Cs-USY using TMAOH 1 M solution as solvent

3.3. Characterization techniques

3.3.1 Thermogravimetric analysis (TGA)

Thermal analysis allows monitoring mass variations in a material as a function of temperature while a controlled temperature program is running. This is very useful for reactions involving mass loss (drying, reduction, desorption, and degradation) or mass gain (adsorption, wetting, and oxidation) and especially for solid-gas systems. Measurements in either inert or reactive gas atmosphere are possible over a wide temperature range using a constant heating rate. [62]

So, in present work, TGA analysis was used mainly for two purposes:

- Determine the amount of water adsorbed over the samples after saturation with water so that the same dry amount of catalyst could be used for each catalytic test;
- Study the strength of the interaction between water and the materials in order to estimate the hydrophobicity index (h), defined as the ratio between the water mass losses verified at 150 ^{0}C and 400 ^{0}C over the saturated zeolites [63].

$$\mathbf{h} = (\mathbf{Mass\ loss\ at\ 150\ ^\circ C})/(\mathbf{Mass\ loss\ at\ 400\ ^\circ C}) \qquad \mathbf{(2)}$$

In this work a Setsys Evolution TGA from Setaram instruments was used to perform TGA-DSC analysis. For each experiment, a mass of catalyst around 30 mg was used. A heat treatment was applied from 20 to 400 °C using a rate of 10 °C/min and a gas (air in all cases except for sol-gel samples, where nitrogen was used) flow of 30 ml min^{-1}. This heat treatment was done twice in a manner that result from the second cycle were subtracted in the first cycle to eliminate the possible error or noise. The scheme for the temperature program used in TGA-DSC experiments can be seen below.

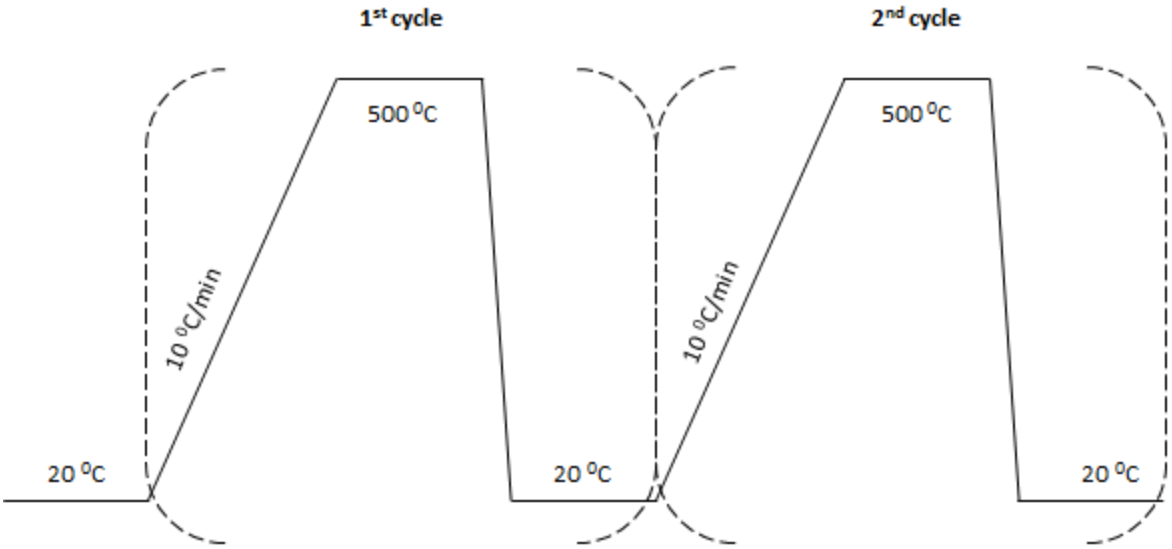

Figure 9: Temperature program profile used during TGA-DSC analysis.

3.3.2 X-Ray diffraction (XRD)

X-Ray diffraction (XRD) is a technique commonly applied in zeolites for the identification of the framework type and the chemical composition [64]. Indeed, from an XRD experiment, one can learn if sample is crystalline and how many and which crystalline phases are present [62].

Basic equation which governs the principle behind X-ray diffraction is Bragg's equation. Bragg's diffraction occur only if the scattered rays constitutes the constructive interference i.e. path difference between two scattered rays from 1st and 2nd layer of atoms of crystal material is equal to the integral multiple 'n' of wavelength λ. The path difference between two waves undergoing interference is given by Bragg's Law, where n is the diffraction order, d is interatomic distance, λ wavelength of incident wave, and θ is the diffraction angle. [62].

$$n\lambda = 2d\sin\theta \qquad (3)$$

In this work, powder X-ray diffraction was used to get information about the types of phases present on the prepared catalysts and to estimate average NiO/Ni^0 sizes through Scherrer equation. Powder XRD patterns were obtained in a Bruker AXS Advance D8 diffractometer equipped with a 1D detector (SSD 160) and using a Ni filter for identifying crystalline phases. The scanning range was set from 5° to 80 ° (2θ), with a step size of 0.03° and a step time of 0.5 s.

3.3.3 Temperature programmed reduction (H_2-TPR)

Temperature programmed reduction (H_2-TPR) is a useful technique to characterize metallic catalysts in terms of reducibility properties [62]. In these experiments, samples are placed in a reducing atmosphere and H_2 is circulated through the catalyst bed while the temperature is varied linearly. H_2 consumption as a function of temperature is continuously monitored through TCD detectors. Resulted TPR profiles reflect the ability of metal species to get reduced, providing also information regarding metal species nature and location in the used support [65].

In the present work, H_2-TPR tests were carried out in a Micromeritics AutoChem II using around 0.150 g of catalyst in every experience. At first, catalysts were pre-treated under argon flow (25 ml min^{-1}) at 250 ^{0}C for 1 h, with a ramp of 10 °C/min, and then cooled down to the room temperature. Then, TPR was carried out by flowing 30 ml min^{-1} of a 5%H_2/Ar flow and raising the temperature from room temperature to 900 °C, at 10 °C/min, as shown in Figure 10.

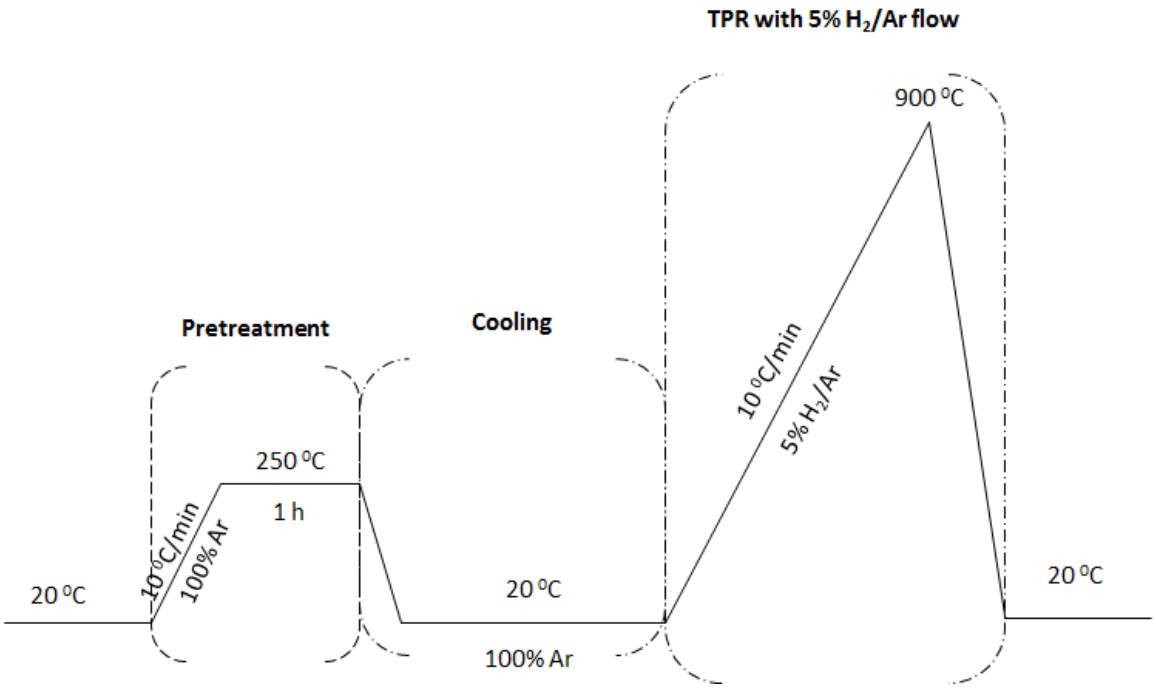

Figure 10: Scheme of the H_2-TPR procedure.

3.4. Catalytic tests

3.4.1 Experimental setup

The scheme for the catalytic setup used in the evaluation of catalytic performances is shown in Figure 11 . The samples were placed in reactor, where a thermocouple was inserted close to the catalyst bed and positioned inside a TermoLab electric oven connected to a temperature program controller. All Gases (N_2, H_2, and CO_2) were supplied by Air Liquid with purities above 99.999% and regulated using mass flow controllers supplied by Brooks.

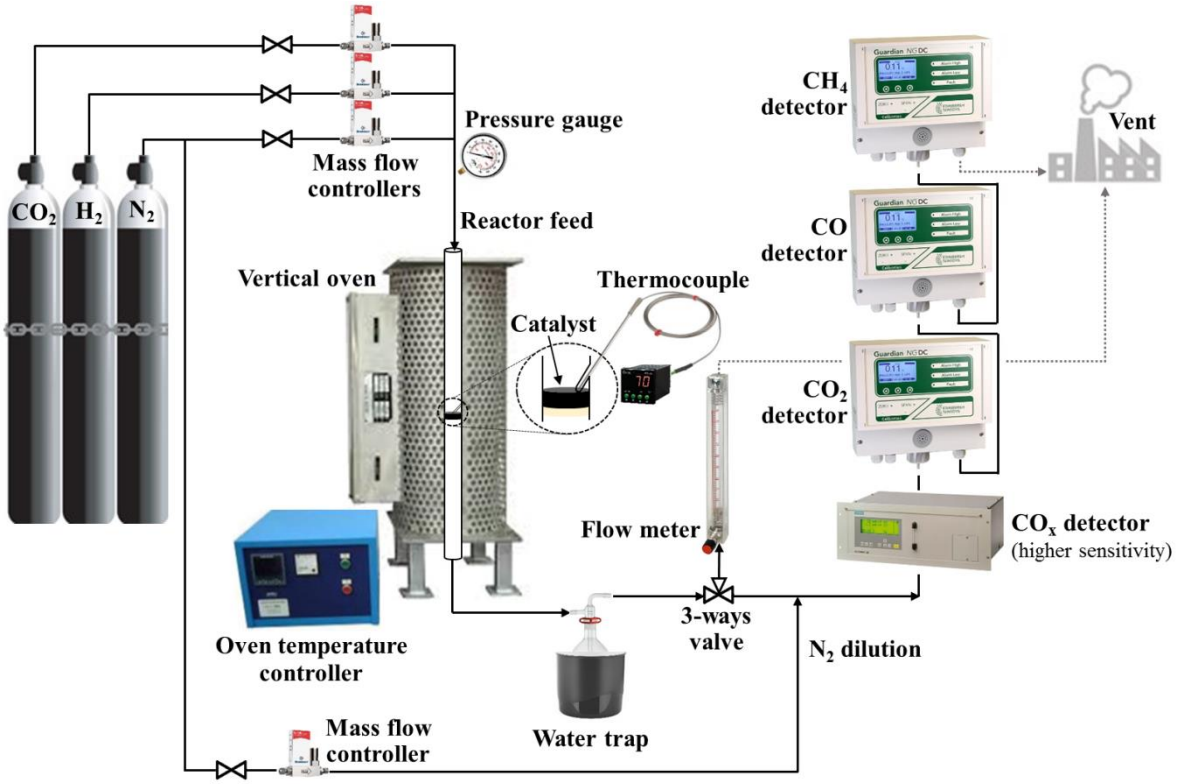

Figure 11: Scheme for catalytic test.

3.4.2 Operating conditions

Catalytic tests were performed using a fixed mass of catalyst (0.200 g) at atmospheric pressure. The temperature profile regarding the tests can be found in Figure 12. As seen, in-situ pre-reduction was generally performed at 470 ^{0}C for 1 h (heating rate of 2.5 ^{0}C min^{-1}) with 80%H_2/20%N_2 flow of 250 ml min^{-1} to get metallic Ni^0 species. In some specific cases (e.g. 15% Ni/Cs-$USY_{2\text{-Propanol}}$ and sol-gel catalysts) the effect of the pre-reduction conditions were evaluated. Indeed, for 15% Ni/Cs-$USY_{2\text{-Propanol}}$ a test was performed after reducing at 650 °C to evaluate the effect of this parameter in the amount of reduced metallic species, average particle size and catalytic performances obtained while,

in case of sol-gel samples, tests were performed with and without in-situ pre-reduction. Catalytic tests were performed between 250 and 450 ^{0}C keeping a reaction feed gas of H_2, CO_2 and N_2 at a molar ratio of 36:9:10 (stoichiometric ratio between H_2 and CO_2, total flow = 290 ml min^{-1}). For each reaction temperature, after stabilization of catalytic system average value of the required data was taken for calculation of CO_2 conversion and CH_4 methane selectivity.

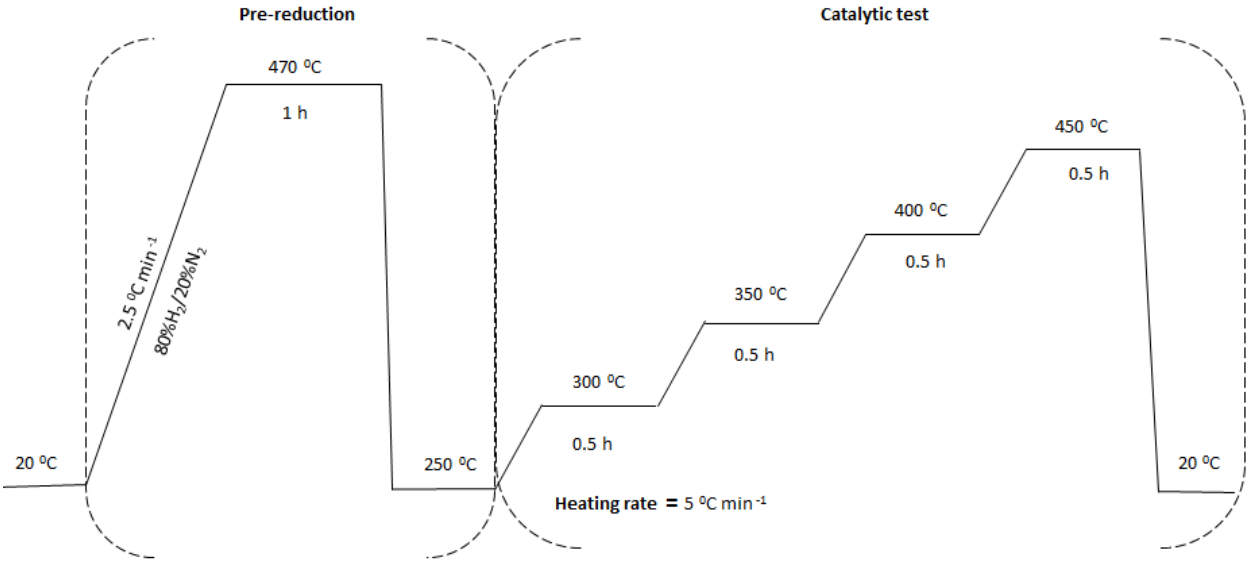

Figure 12: Temperature program used for carrying out catalytic tests.

3.4.3 Determination of the CO_2 conversion and CH_4 selectivity

Conversion of a reactant called A is calculated as the ratio of the moles of A converted per unit time to the molar flow rate of A fed and multiplied by 100. So, in terms of CO_2 as a reactant for methanation reaction, conversion can be defined as:

$$\textbf{CO}_2\textbf{ conversion (\%)} = \frac{F_{CO_2,inlet} - F_{CO_2,outlet}}{F_{CO_2,inlet}} * 100 \qquad (4)$$

Furthermore, selectivity of the desired product B is defined as percentage (%) of A which reacted to give B. Thus, in case of methanation reaction, the selectivity to CH_4 (and CO) were calculated as shown below:

$$\textbf{CH}_4\textbf{ selectivity (\%)} = \frac{F_{CH_4,outlet}}{F_{CO_2,inlet} - F_{CO_2,outlet}} * 100 \qquad (5)$$

$$\textbf{CO selectivity (\%)} = \frac{F_{CO,outlet}}{F_{CO_2,inlet} - F_{CO_2,outlet}} * 100 \qquad (6)$$

The detailed calculation of the conversion and selectivity for a certain $T_{reaction}$ can be found in Annex I.

4. Results and discussion

In order to properly discuss the results obtained through the application of the three strategies presented in the Experimental part regarding the promotion of Ni dispersion on zeolite-based catalysts for CO_2 methanation, this chapter was divided into three sub-chapters dealing with the promoter's incorporation, the impregnation solvent effect and the application of sol-gel method.

4.1 Promoter nature effect

In this section, results regarding the effects of the promoter nature in bimetallic 15%Ni-15%M/Cs-USY catalysts (Table 2) will be discussed and analyzed in terms of characterization results and catalytic performances.

Catalysts characterization

Firstly, **thermo-gravimetric analysis (TGA)** was performed for all samples presented in Table 2 after saturation with water since, as already referred, this characterization technique can be used to check the strength of the water-zeolites interactions through h index calculation. As previously discussed, if a zeolite is highly hydrophilic then h index will be close to 0 while, for more hydrophobic materials, h values will be close 1. According to the results presented in Figure 13 and Table 5, one can notice that the nature of the added promoter does not significantly affect the hydrophobic properties of the materials. Indeed, h indexes close to 0.80 were obtained for the different catalysts from the present chapter, being these values in accordance with the obtained in the literature for similar samples [29]. Even if samples present a similar behavior in terms of the interaction with water, yttrium seems to lead to a slightly higher hydrophilic surface, as seen by the deviation found in the h index when comparing with the rest of materials. Moreover, all the samples presented similar water mass losses, being the endothermic reaction leading to this variation in the mass achieved below 400 °C for all the materials.

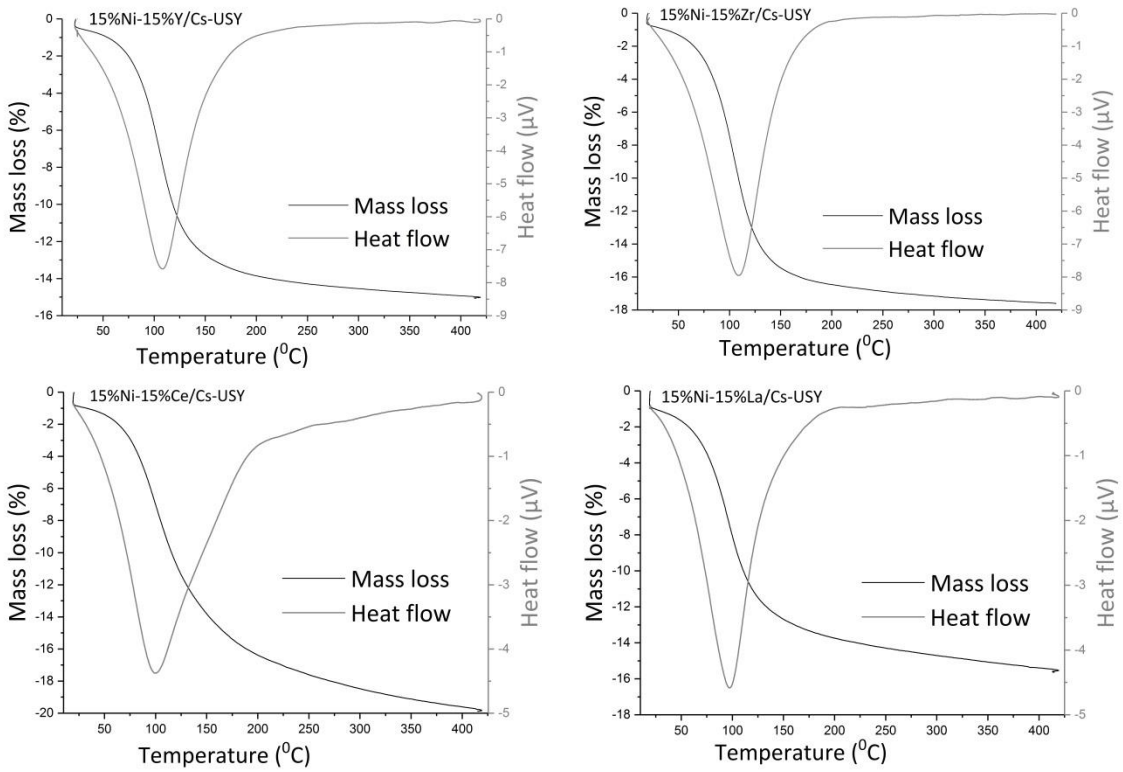

Figure 13: TGA profiles of promoted samples.

Table 5: h indexes and average particle sizes obtained for the 15%Ni-15%M/Cs-USY samples of this work.

Catalysts	h index	ØNiO (nm)	$ØNi^0$ (nm)
15%Ni-15%Ce/Cs-USY	0.85	<5	<5
15%Ni-15%Zr/Cs-USY	0.88	24	20
15%Ni-15%La/Cs-USY	0.82	27	23
15%Ni-15%Y/Cs-USY	0.70	9	10

To follow the study, **XRD diffractograms** were collected for the 15%Ni/Cs-USY_{Water} and 15%Ni-15%M/Cs-USY samples before and after reduction (Figure 14). For comparison purposes, Cs-USY zeolite support pattern was also collected. As it can be clearly seen, all samples present the characteristic peaks of Faujasite (FAU) structure in range of 2θ = 5-45°, characterized by the main

diffraction peaks at 2θ = 6.398°, 15.768° and 23.718°, indicating that zeolite structure was preserved even with metal loading via co-impregnation [66][19]. However, the zeolite peaks intensity decreases with the incorporation of the metals, which could be due to the formation of some amorphous phases after the metal loading or even due to the adsorption of X-rays by the promoter species incorporated. Regarding the nature of the incorporated Ni species, on one hand, in the calcined samples diffraction peaks 2θ = 37 °, 43 ° and 63 ° are found, being them attributed to the presence of NiO phases [19][67]. On the other hand, for the reduced samples, no diffraction peaks attributed to NiO are found, and three peaks corresponding to metallic nickel phases can be observed at 2θ = 44.5, 51.8, 76.3 ° [68][67]. To be remarked is that, for Ni-Ce sample, a significant decrease of all peaks intensities can be observed. This could be due to very small particle sizes (increased dispersion) or to the high X-ray absorption coefficient for Ce [19]. Additionally, no peaks attributed to Ce oxides (2θ = 28.6, 33.3 and 47.5° [19]), Zr oxides (2θ = 28.4, 30.2, 35.2, 50.3 and 60.2° [68]), La oxides (2θ = 25, 34 and 57 ° [50]) nor Y oxides (2θ = 29.3, 34.0, 48.8 and 57.9° [69]) were found in the samples, what could be ascribed to a high dispersion of the metal promoters over the structure. Complementarily, by applying Scherrer equation, the average sizes of NiO/Ni^0 particles in the studied samples were estimated (Table 5). As observed, particle sizes varied following the order: Ni-Ce < Ni-Y < Ni-Zr < Ni-La. Consequently, more dispersed Ni species are expected over Ce and Y-containing catalysts, what could eventually lead to higher catalytic performances.

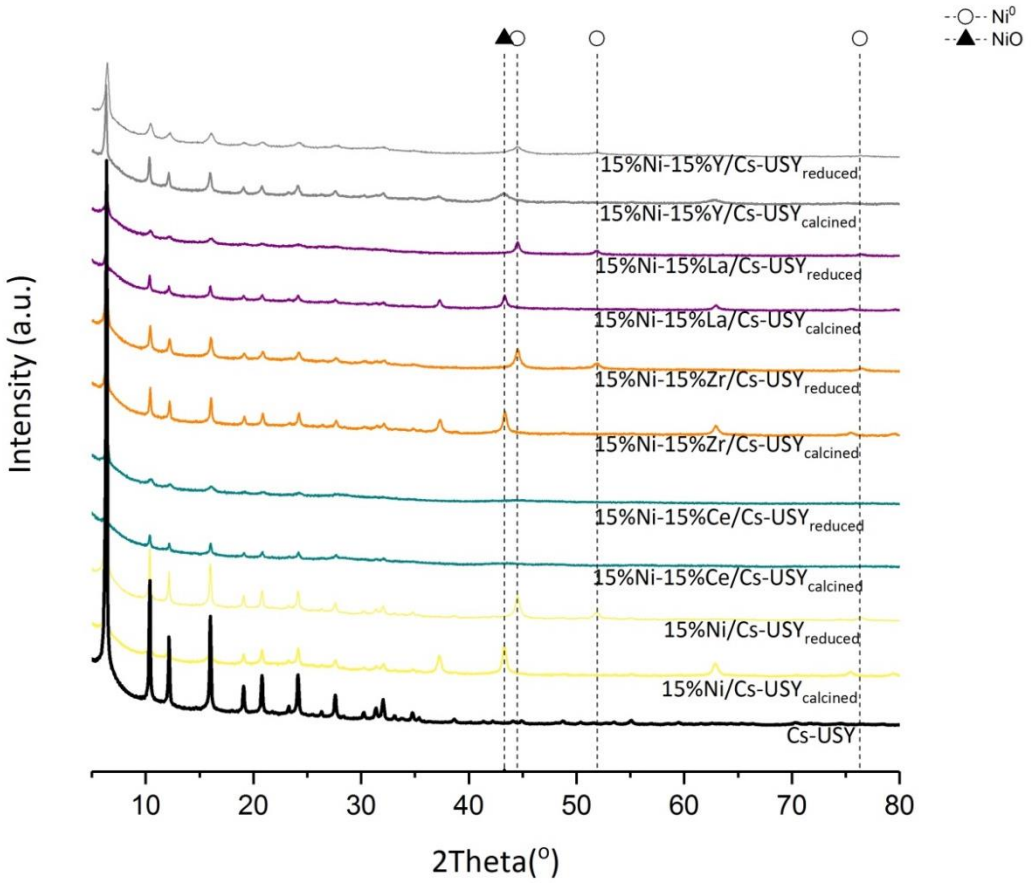

Figure 14: XRD pattern of promoted samples with support (Cs-USY).

Furthermore, in order to determine the reduction profiles of the samples with different promoters, **H_2-TPR** experiments were carried out (Figure 15). For comparison purposes, the profile obtained for the equivalent monometallic sample (15%Ni/Cs-USY_{Water}) is also presented. As observed, H_2 consumption peaks appear in all samples in the range of 250 to 750 °C. Reduction peaks present at 250-400 °C can be typically attributed to the reduction of NiO species located on the external surface of zeolites, presenting weak interaction with the support [19]. However, in case of the bimetallic catalysts, new reduction processes seem to occur. To be pointed out is that, in samples with Y and Ce, a great fraction of NiO species is observed to be present in the cavities of zeolites due to presence of highly dispersed metal oxides phases as verified with XRD result (Table 5). Indeed, the reduction peaks above 500 ^{0}C can be attributed to NiO/Ni^{+2} species located inside zeolites mesopores, supercages, sodalite cages and hexagonal prisms, having strong interaction between metal oxides and support [19]. Taking into account the low Al content of the used zeolite (<1 wt. %), the fraction of Ni species as Ni^{2+} in exchange positions could be considered as negligible. Thus, reduction processes appearing above 500 °C can be ascribed to the reduction of NiO species occluded inside the mesopores present in this specific zeolite (commercially synthesized by dealumination) [29][30].

Additionally, temperature shifts on the peaks maxima with respect to the monometallic sample (15%Ni/Cs-USY$_{Water}$) can be observed with the incorporation of some promoters (e.g. Ce, Y), suggesting the establishment of synergistic interactions between Ni and the promoters, which create new levels of metallic interactions. However, in the catalysts with Zr and La, not such remarkable differences can be observed, which could indicate that the addition of these promoters does not modify significantly NiO species reducibility [49]. The chosen pre-reduction temperature for the catalytic tests was, in accordance with previous studies, 470 ^{0}C. As seen, a great fraction of Ni species will be reduced at this temperature for all the samples.

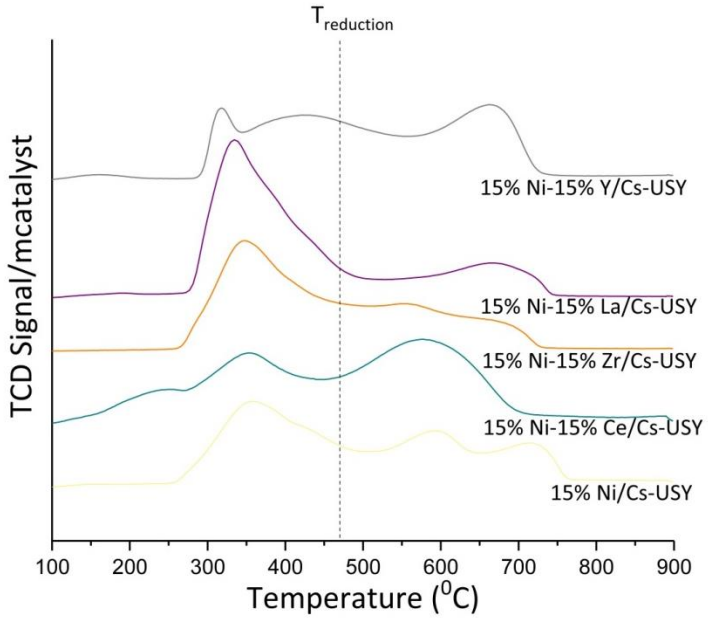

Figure 15: H_2-TPR profiles of promoted samples.

Catalytic tests

Finally, the bimetallic catalysts whose main properties were previously discussed were tested under CO_2 methanation conditions. Thus, Figure 16 shows CO_2 conversion and methane selectivity obtained at temperatures ranging from 150 to 450 °C for the samples under analysis. It can be observed that the un-promoted 15% Ni/Cs-USY$_{Water}$ catalyst exhibits generally lower CO_2 conversion and selectivity than the bimetallic catalysts. This result confirms that catalysts performances can be boosted by incorporating the proper promoters through the enhancement of the particle sizes and the potential contribution in the methanation mechanism as CO_2 activation sites. This could lead to a remarkable enhancement of the activity even at low temperatures, where the thermodynamic limitations are not significant. Indeed, one can see that at higher temperatures a similar trend is observed for all the

samples only with the exception of the catalyst promoted with Zr, which presented results similar to those of the monometallic sample, likely due to the non-enhanced Ni reducibility (Figure 15) and the not expected participation as carbon dioxide activation site.

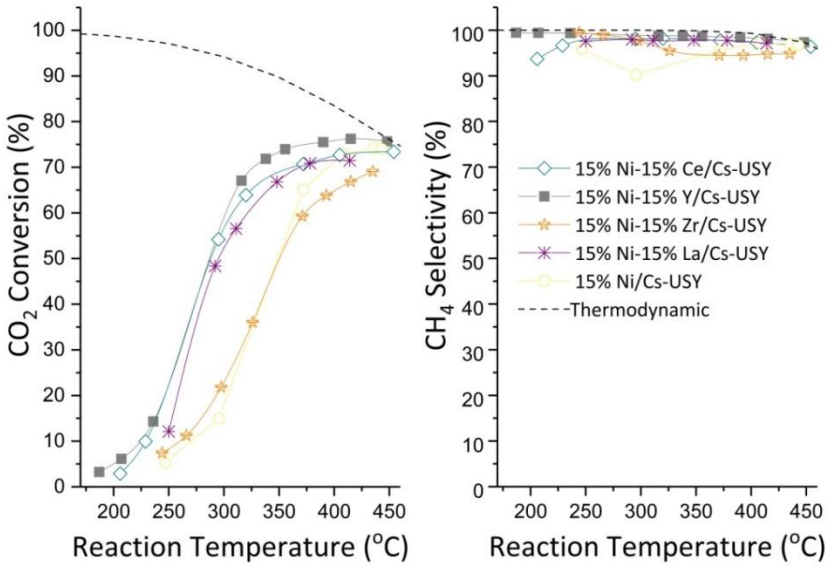

Figure 16: CO_2 conversion and CH_4 selectivity of promoted catalyst at methanation reaction.

In order to clearly study the effects of the different promoters to the activity of the materials towards carbon dioxide methanation, methane yields determined for the bimetallic samples at three representative temperatures are depicted in Figure 17. Thus, it can be seen that results followed the trend: Ni-Y > Ni-Ce > Ni-La >> Ni-Zr. As seen, yttrium remains as the most favorable promotor, followed by cerium, which could be due to the favored particle sizes (Ni^0) as verified with XRD characterization (Table 5) and the enhanced reducibility of NiO species [69][70], without excluding a possible effect of Y in the number of CO_2 activation sites. In specific case of Ce, the improvement of the catalytic performances can be also attributed to the well-known oxygen vacancies present in the structure due to existence of Ce oxides species like Ce_2O_3 and CeO_2 which could aid in CO_2 adsorption sites [49]. Furthermore, the lower methane yields observed for La and Zr containing catalysts could be due to the lower Ni reducibility in these samples, as reported in the literature [49] and also verified from H_2-TPR results (Figure 15), and also to the larger Ni^0 particles present in these samples, as seen by the analysis of XRD diffractograms.

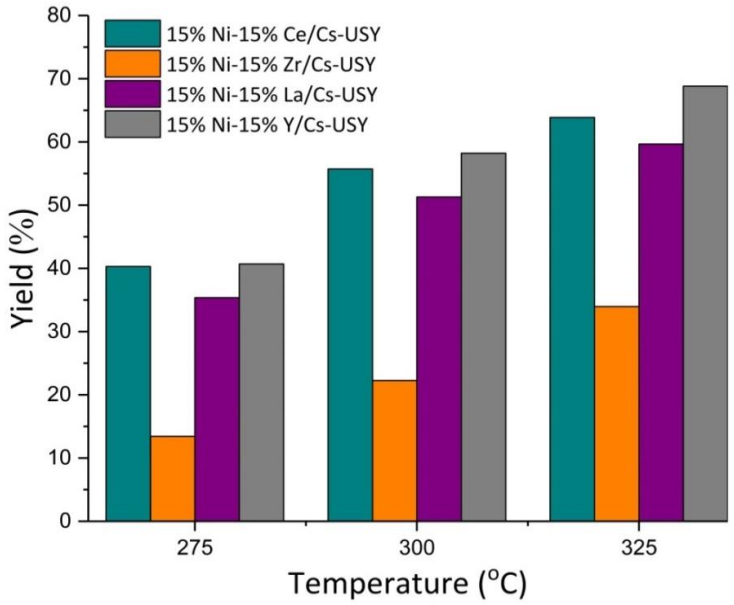

Figure 17: Methane yield of different promoted catalyst

In order to further investigate the properties of these bimetallic catalysts, XRD of spent samples are presented in Figure 18.

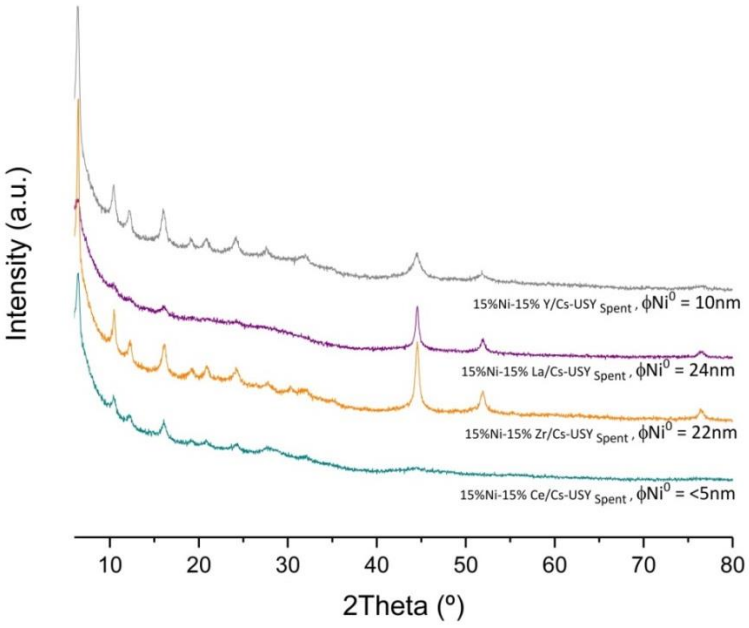

Figure 18: XRD of spent samples

As already discussed, it can also be observed here that the promoted samples again proved resistance towards sintering as verified from the Ni^0 particle sizes obtained for spent samples. Moreover, regarding zeolite structure, it can also be seen that the structure is still preserved in most

of the samples related with this study indicating the positive characteristic of promoter incorporation.

In order to further complete this study, Figure 19 compares the results obtained for the sample containing the best promoter (yttrium) with a commercial hydrogenation catalyst (Ni/γ-Al_2O_3) tested under the same reaction conditions. As it can be easily observed, the promoted zeolite catalyst presents even better results than the commercial even at low temperatures, being the CO_2 conversion ~73% and the CH_4 selectivity ~99 % at 350 ^{0}C when compared to the commercial catalyst with CO_2 conversion ~63% and CH_4 selectivity ~98% at the same reaction temperature.

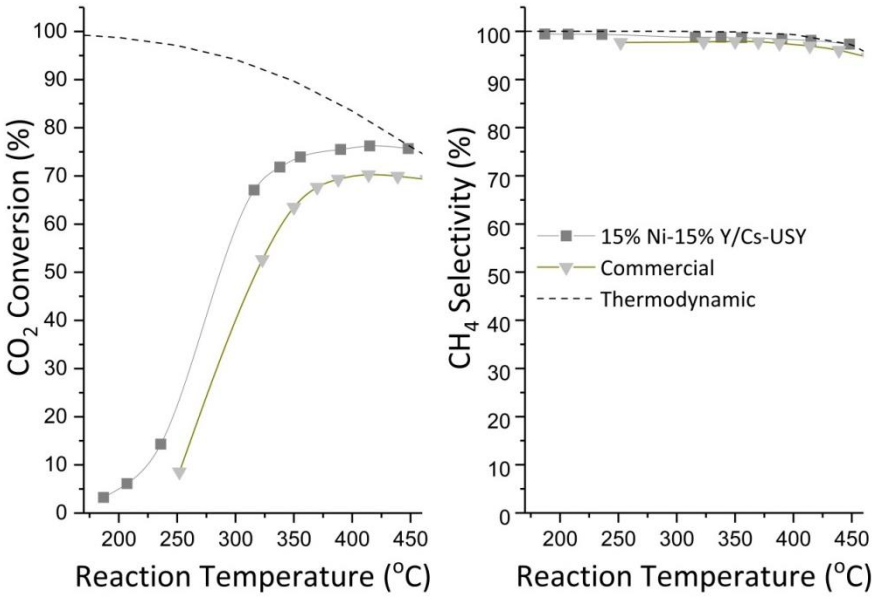

Figure 19: Comparison of best promoter with commercial catalyst.

4.2 Impregnation solvent effect

In this second study, the effect of tuning the impregnation solvent used in the preparation of 15% Ni/Cs-$USY_{Solvent}$ catalysts (Table 3) will be analyzed both in terms of characterization and catalytic performances.

Catalysts characterization

As done for the bimetallic samples, **thermo-gravimetric analysis (TGA)** was performed for the catalysts presented in Table 3 after the corresponding saturation with water. As observed in Figure 20 and Table 6, the nature of the impregnation solvent does not lead to significant changes in the hydrophobic properties of the materials, with h indexes of ~0.95 in all samples. Thus, the strong

hydrophobic nature of the zeolite support seems to be preserved. Also, similar mass loss behavior is also observed for the different samples.

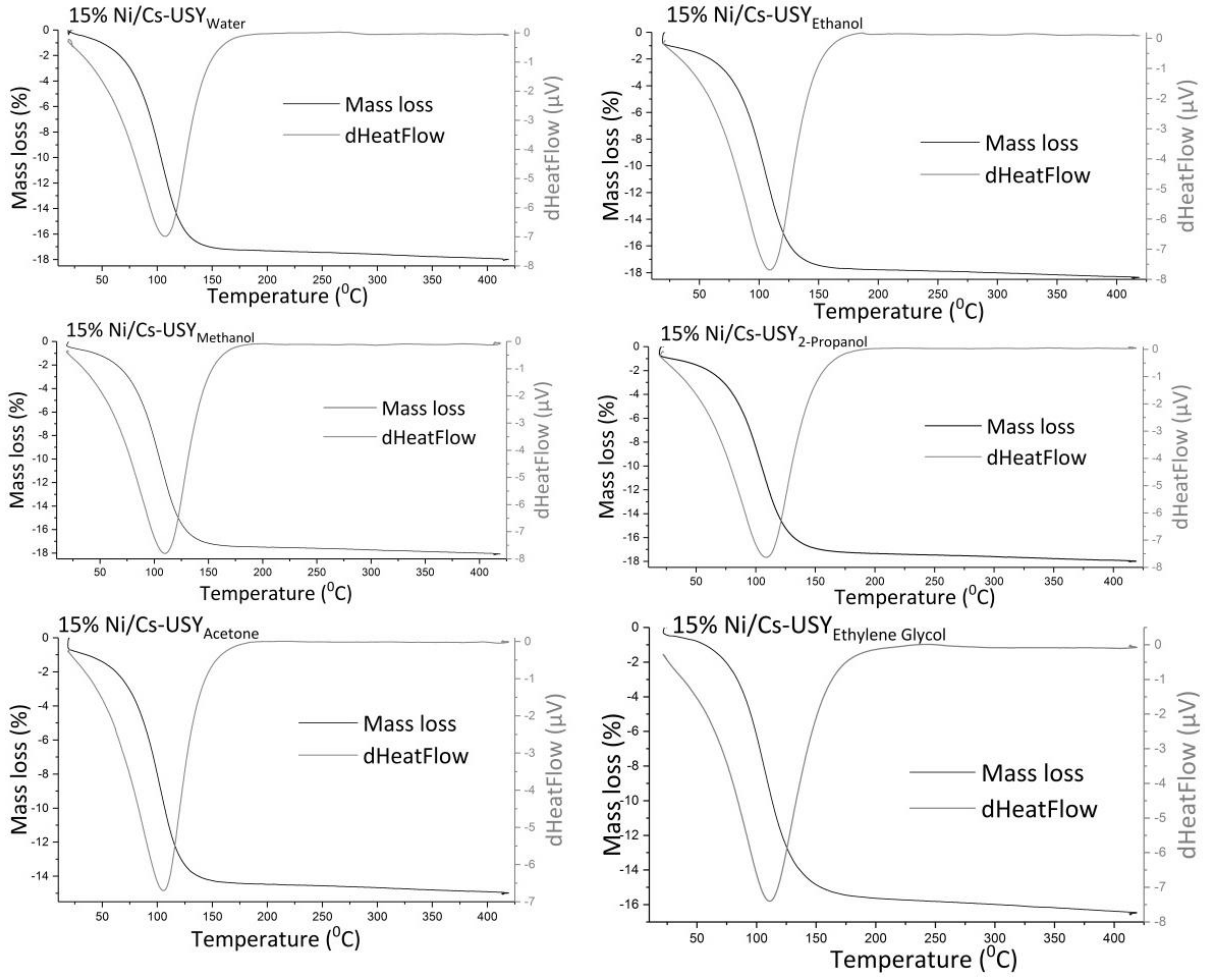

Figure 20: TGA profiles of mono-metallic samples with different impregnation solvent.

Table 6: h indexes, average particle sizes and crystallinities obtained for the 15Ni/Cs-USY$_{Solvent}$ samples of this work.

Catalysts	h index	ØNiO (nm)	ØNi^0 (nm)	Crystallinity after reduction (%)
15% Ni/Cs-USY$_{Water}$	0.95	22	19	70
15% Ni/Cs-USY$_{Ethanol}$	0.95	23	21	67
15% Ni/Cs-USY$_{Methanol}$	0.95	21	17	66
15% Ni/Cs-USY$_{2\text{-}Propanol}$	0.94	17	13	65
15% Ni/Cs-USY$_{Acetone}$	0.96	23	22	71
15% Ni/Cs-USY$_{Ethylene\ glycol}$	0.91	7	13	43

Also, **XRD patterns** obtained for the samples prepared using different impregnation solvents, before and after calcination, are shown in Figure 21.

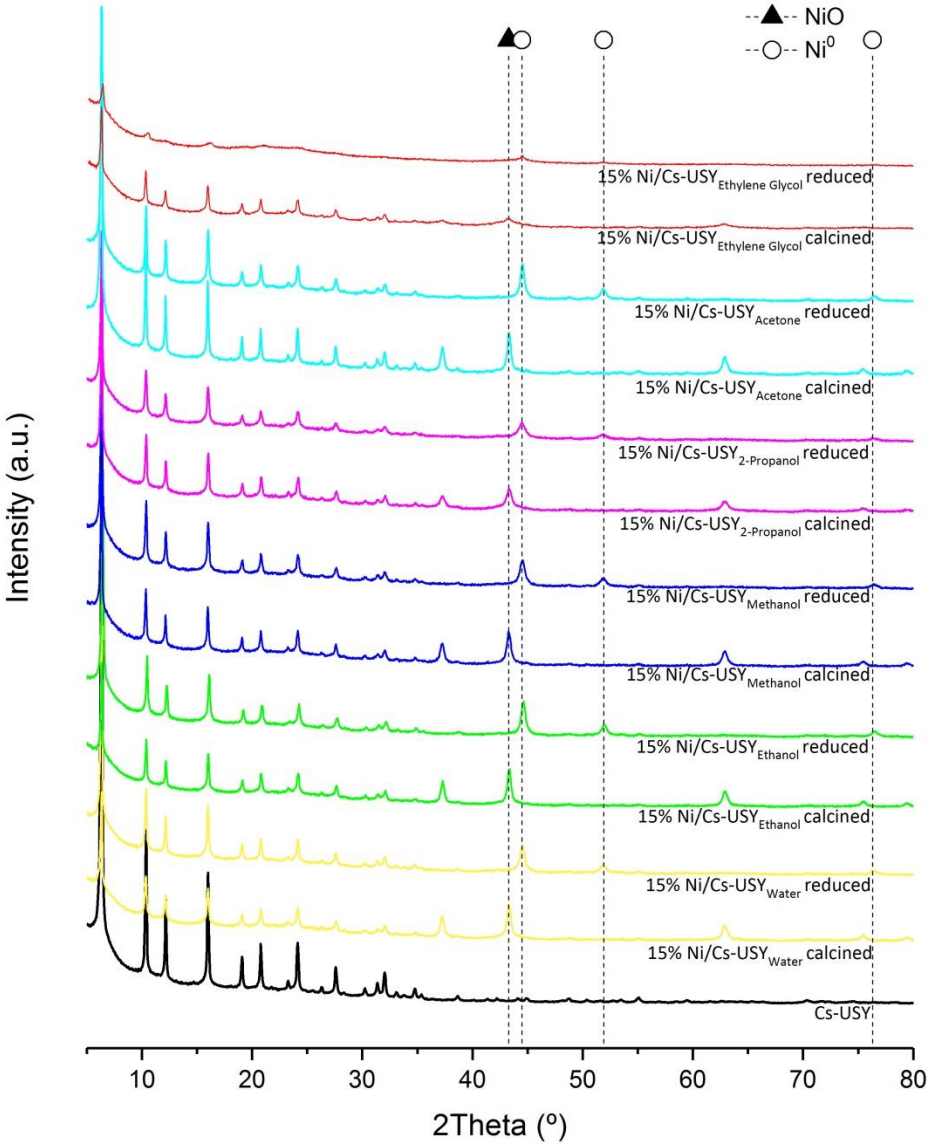

Figure 21: XRD of samples with different impregnation solvents

As seen, zeolite structure is still preserved irrespective of the solvent used with the exception of ethylene glycol sample, where zeolite characteristic peaks intensity significantly decreases with the thermal treatments, indicating the damage of the structure, as confirmed by the crystallinities presented in Table 6. Moreover, regarding the presence of Ni species, NiO (2θ = 37 °, 43 ° and 63 ° [19][67]) and Ni^0 (2θ= 44.5°, 51.8° [68][67]) phases peaks could be confirmed in most of the catalysts

after calcination and reduction, respectively. Again, in case of ethylene glycol, NiO/Ni^0 peaks are less intense, suggesting a highly dispersed metallic phase. As previously done, by applying Scherrer equation the average particle sizes after calcination and reduction were determined for all samples (Table 6). According to the obtained results, 2-propanol and ethylene glycol samples present the smallest Ni^0 particles, followed by methanol, water, ethanol and acetone. To be remarked is that, while for most of the samples the variation between the NiO and Ni^0 sizes is similar (2-4 nm), in the ethylene glycol sample the occurrence of severe sintering processes during the pre-reduction treatment is evident as the particle size doubles.

Regarding **H_2-TPR** profiles (Figure 22), peaks with stronger and weaker interactions of Ni species with the support can be observed. As previously discussed, H_2 consumption peaks below 500 ^{0}C could be attributed to the reduction of NiO species dispersed onto external surface of the zeolite support while reduction peaks above 500 ^{0}C could be ascribed to the reduction of NiO located inside the mesopores present in this zeolite [29][30]. As seen, the nature of the impregnation solvent used presents an impact in the reducibility properties of the synthesized catalysts. Indeed, samples with smaller NiO particles according to Table 6 (e.g. 2-propanol, ethylene glycol) present greater reduction processes at 550-750 °C. This behavior is somehow expected as the smaller particles could be easily located inside the cavities present in the zeolite, while agglomerated NiO particles will tend to be located in the external surface.

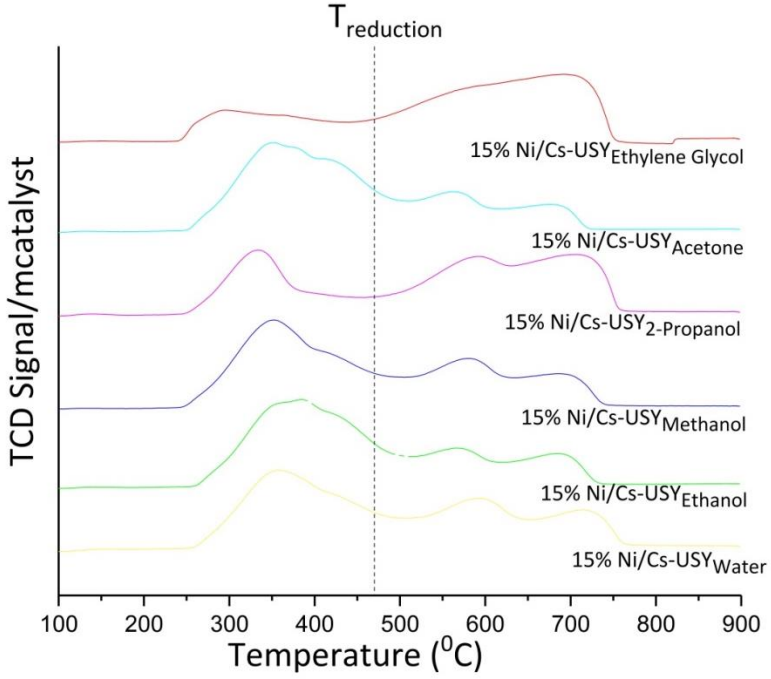

Figure 22: H_2-TPR profiles of samples with different impregnation solvents.

Catalytic tests

The catalytic performances obtained for the catalysts previously analyzed are presented in Figure 23. Indeed, one can observe that the nature of the impregnation solvent affects the obtained CO_2 conversions and also the selectivity to methane. In fact, the catalyst presenting the better performances is the one prepared using 2-propanol as solvent, followed by ethylene glycol and then catalysts impregnated with water, methanol, ethanol and acetone. These findings are generally in well accordance with their XRD results in terms of Ni^0 particle sizes (Table 6).

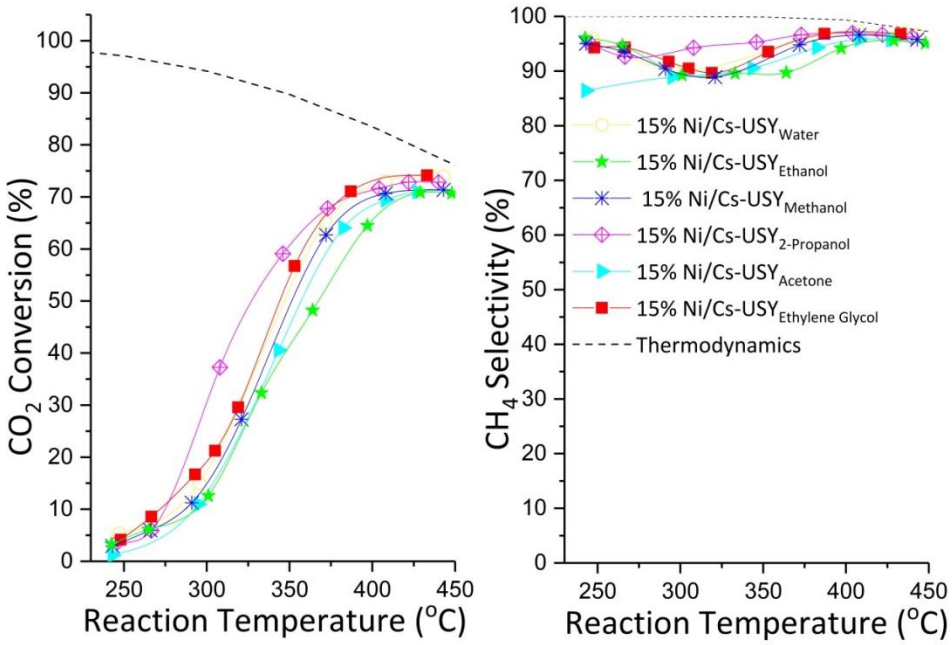

Figure 23: CO_2 conversion and CH_4 selectivity of impregnated catalyst at methanation reaction condition

However, in order to have clearer picture of catalytic performances for the samples prepared with different solvents, a bar graph presenting methane yields of the samples at three representative temperatures is presented in Figure 24. There, it can be clearly seen that the highest methane yield is provided by the use of 2-propanol. However, the results of ethylene glycol are lower than the expected when analyzing the particle size and reducibility of Ni species in this catalyst. Indeed, one can explain these unexpected results by the structural damage produced in the zeolite during the pre-reduction treatment, according to the crystallinity value previously presented in this work.

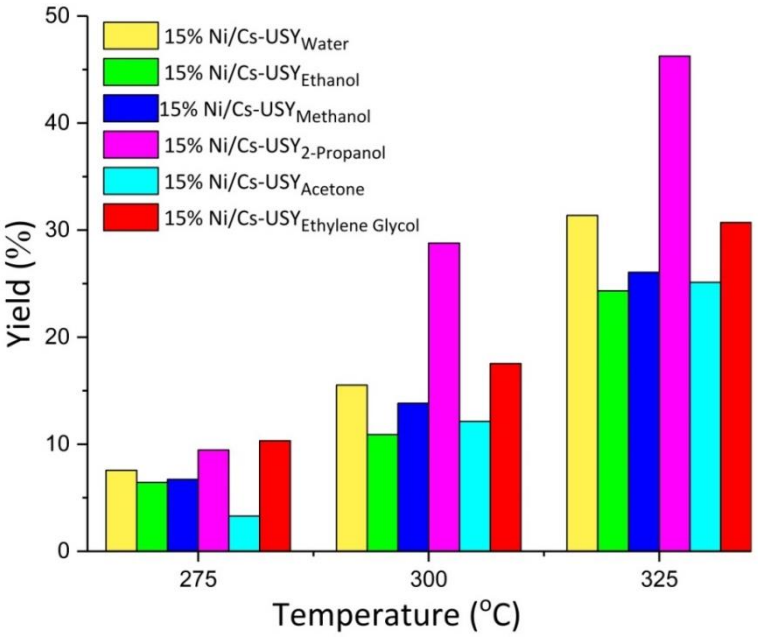

Figure 24: Methane yield of different impregnated catalyst

To further investigate the samples, XRD diffractograms of spent catayst are shown in Figure 25 .

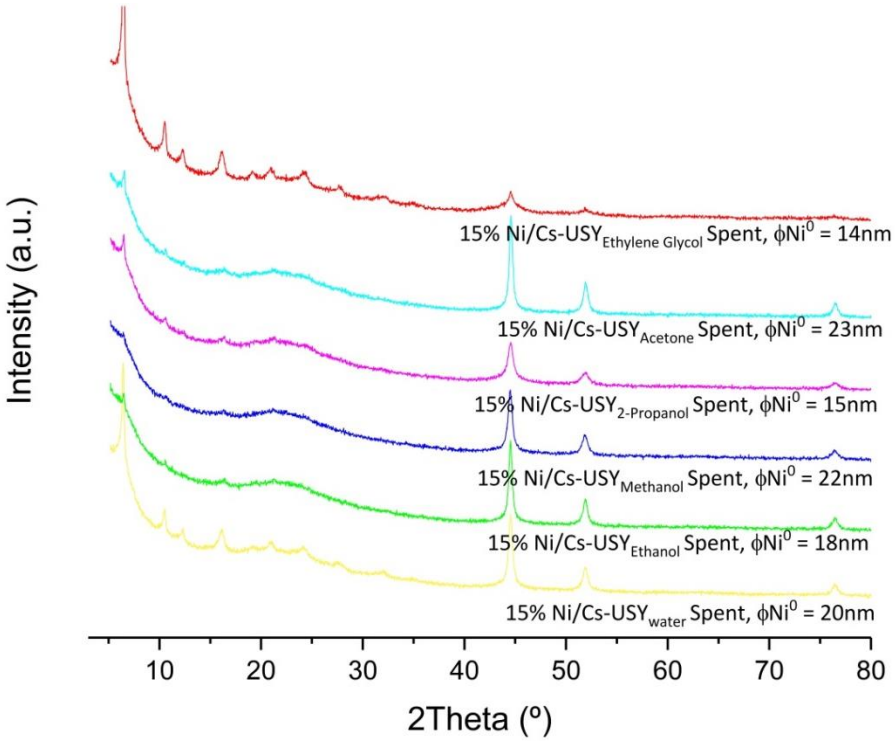

Figure 25: XRD of the spent 15 wt.% Ni samples prepared with different impregnation solvents.

Despite of the positive effect of the impregnation solvent in metal dispersion, structural damage can be observed in most of the samples. This effect could be, according to some works of the literature

where authors verified changes in zeolites structure type with the use of different cations, due to the formation of Cs-OH species during the thermal treatment which could result in to the structural damage of FAU zeolite.

Finally, as a complementary study, being the sample prepared using 2-propanol the one leading to the best performances and presenting this catalyst a significant fraction of unreduced NiO species at high temperatures according to the H_2-TPR profiles, the effect of the pre-reduction temperature on the catalytic performances of this sample was also studied. For this purpose, an additional catalytic test was carried out after performing a pre-reduction treatment at 650 °C and the obtained results were compared to those from the previously reported experience (with reduction at 470 °C). As it can be observed from Figure 26, the catalytic performances are not significantly affected by the pre-reduction temperature, despite the expected increase of the fraction of reduced Ni species. As already reported in the literature [26][29][30], increasing the reduction temperature leads to two effects acting in opposite directions; on one side the amount of reduced Ni species increases, leading to more Ni active sites available for the dissociation of H_2; on the other side, the use of more severe conditions promotes the occurrence of sintering processes, which induces larger particles formation and, consequently, decreases the metallic surface area. Thus, the lack of remarkable effects in the observed performances for this specific catalyst can be again attributed to these opposite effects.

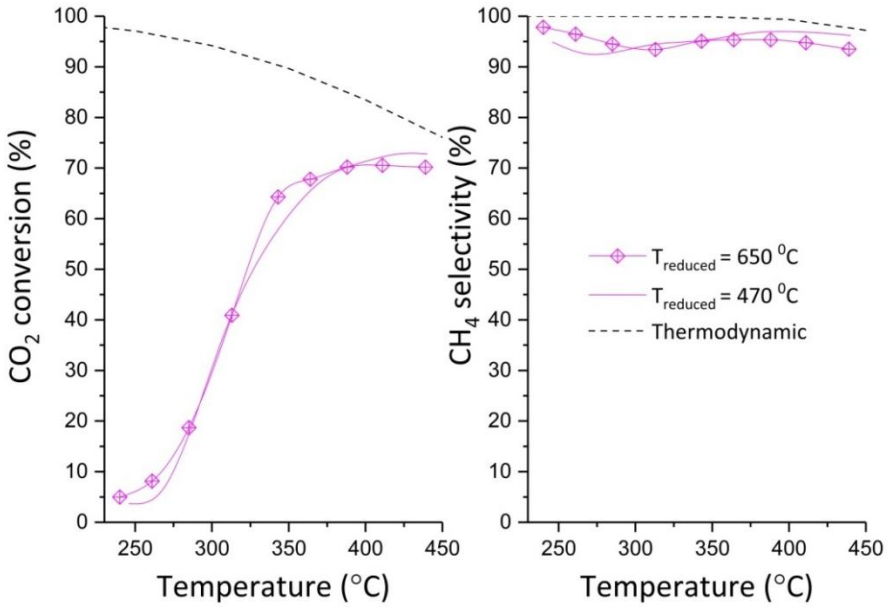

Figure 26: Comparison of catalytic performance of 15% Ni/Cs-USY$_{2\text{-Propanol}}$ reduced at 650 ^{0}C and 470 ^{0}C.

4.3 New Preparation method: Sol-gel

In this section, results of catalysts prepared by Pechini modified method in order to obtain Ni nanoparticles (Table 4) will be analyzed both in terms of characterization and catalytic performances.

Catalysts characterization

Characterization results from **thermo-gravimetric analysis (TGA)** are presented in Figure 27 and Table 7. It can be observed that the sol-gel materials present similar hydrophobic properties, which are directly related with the zeolite support (h index and mass losses) as the pure nickel nanoparticles did not adsorb any water.

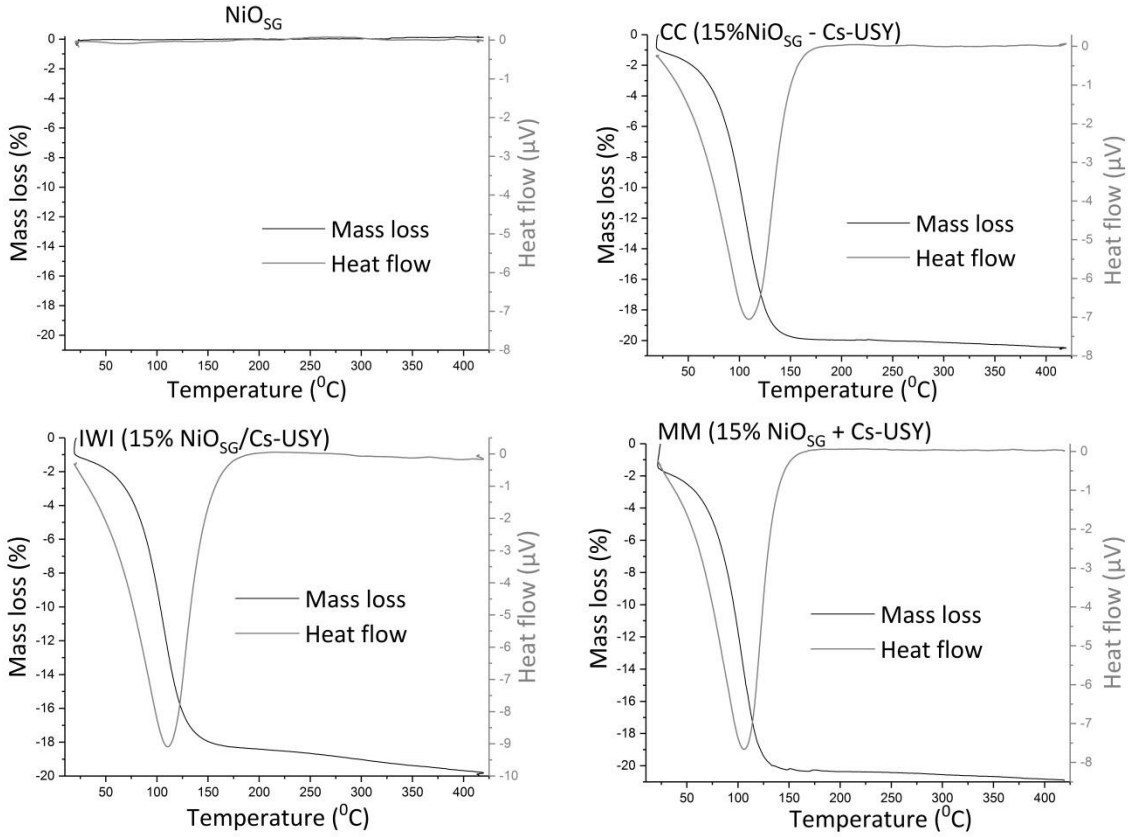

Figure 27: TGA profiles of Sol-gel catalyst

Table 7: h indexes and average particle sizes obtained for the sol-gel samples of the present work

Catalyst	h index	ØNiO (nm)	ØNi^0 $_{calcined\ sample}$ (nm)	ØNi^0 $_{reduced\ sample}$ (nm)
NiO $_{SG}$	-	31	>50	>50
MM [15% NiO $_{SG}$ + Cs-USY]	0.97	31	>50	>50
CC [15% NiO $_{SG}$ - Cs-USY]	0.97	32	>50	>50
IWI [15% NiO $_{SG}$/Cs-USY]	0.91	32	>50	38

The **XRD patterns** obtained for the samples from this chapter after calcination and reduction (Figure 28) reveal the coexistence of NiO and Ni^0 species in the samples prior to the reduction treatment, a fact not verified in any of the previous materials from this work. Indeed, whatever the preparation strategy followed in these sol-gel materials, all samples presented the characteristic diffraction peaks of NiO and Ni^0 after calcination and Ni^0 after reduction. Regarding the effects in the zeolite support, the mechanical mixture and the co-calcination preserve the FAU structure, as its characteristic peaks are observed at 2θ = 6.4, 15.8 and 23.7° [66][19] even after reduction. However, the catalyst prepared by incipient wetness impregnation (IWI) using a TMAOH 1 M solution (for avoiding the agglomeration of the nickel nanoparticles and favoring the formation of a suspension) led to a severe damage in the zeolite, as no peaks can be found in the 5-40 ° region. This effect could be due to the highly basic nature of the used organic solvent tetramethylammonium (TMA), which could result into the solubility of silica species and, hence, the severe structural damage of the FAU zeolite [71]. Furthermore, regarding the Ni species (NiO and Ni^0) particle sizes, in accordance with the higher intensity of their characteristics peaks in the samples from this chapter, very large particles were found in the materials after applying Scherrer equation (Table 7). To be noted is that, despite the destruction of the zeolite structure, the use of IWI hindered the occurrence of severe sintering processes, preserving the particle size of Ni particles after reduction.

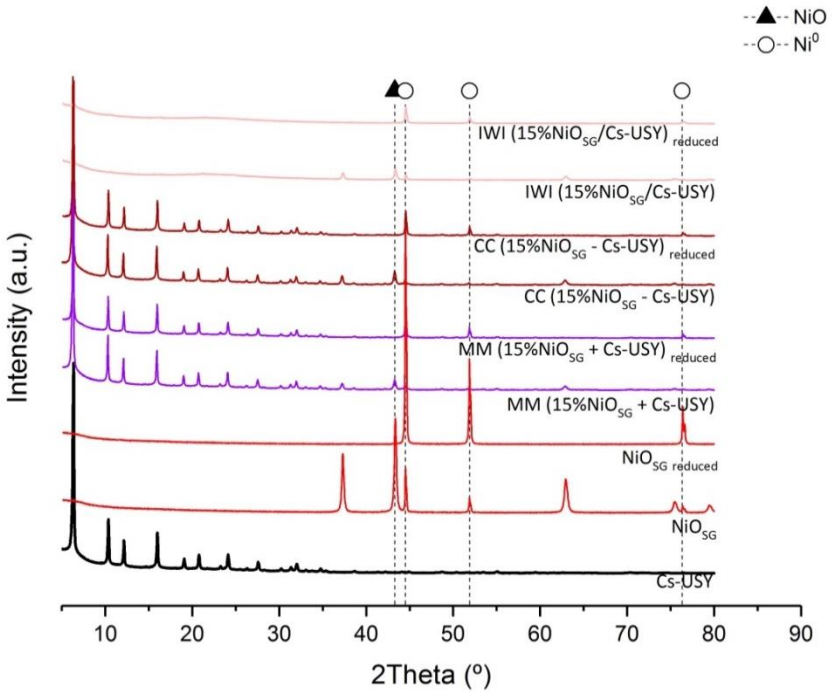

Figure 28: XRD of the Sol-gel samples and Cs-USY.

Regarding **H_2-TPR** profiles (Figure 29), it can be easily observed that the samples prepared by sol-gel method present a unique and prominent reduction process below 500 ^{0}C, indicating that the majority of Ni nanoparticles will be present on the external surface of the zeolite support, with weak metallic-support interactions an probably more prone to sintering issues at higher temperature. According to the H_2 consumptions registered, only 20% of nickel species were presented as NiO in all sol-gel fresh samples (not submitted to any pre-reduction treatment). Consequently, it can be concluded that this preparation method leads mainly (approx. 80%) to the formation of Ni^0 nanoparticles.

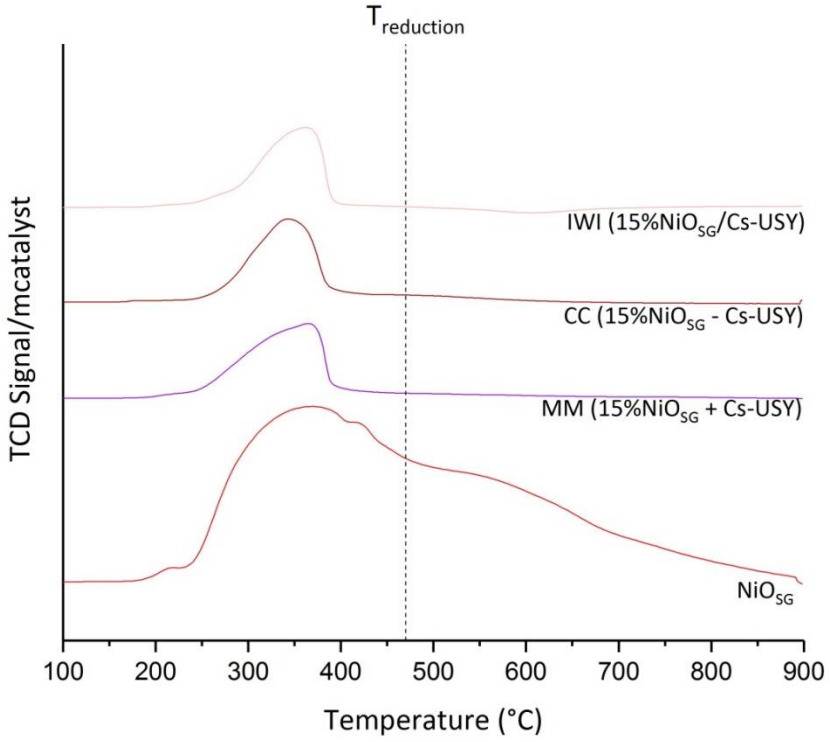

Figure 29: H_2-TPR profiles of Sol-gel catalysts of this study.

Catalytic tests

Regarding the catalytic performances obtained for the samples from this chapter, catalysts were tested both after calcination (as they already presented a great fraction of reduced Ni species according to XRD and H_2 TPR results) and after reduction. In this way, CO_2 conversions are presented in Figure 30 while the selectivities to CH_4 are summarized in Table 8. As observed, the activity of the different materials follows, irrespective of the presence of a pre-treatment, the order: NiO_{SG} > IWI > CC > MM. The considerably higher performances revealed for the unsupported nanoparticles is indeed expected, since the number of Ni active sites was greater in this test (the mass of catalyst per

test was kept constant) with 100 % Ni species in the total sample mass as compared to the other catalysts, which present 15 wt.% Ni and 85% of Cs-based USY support.

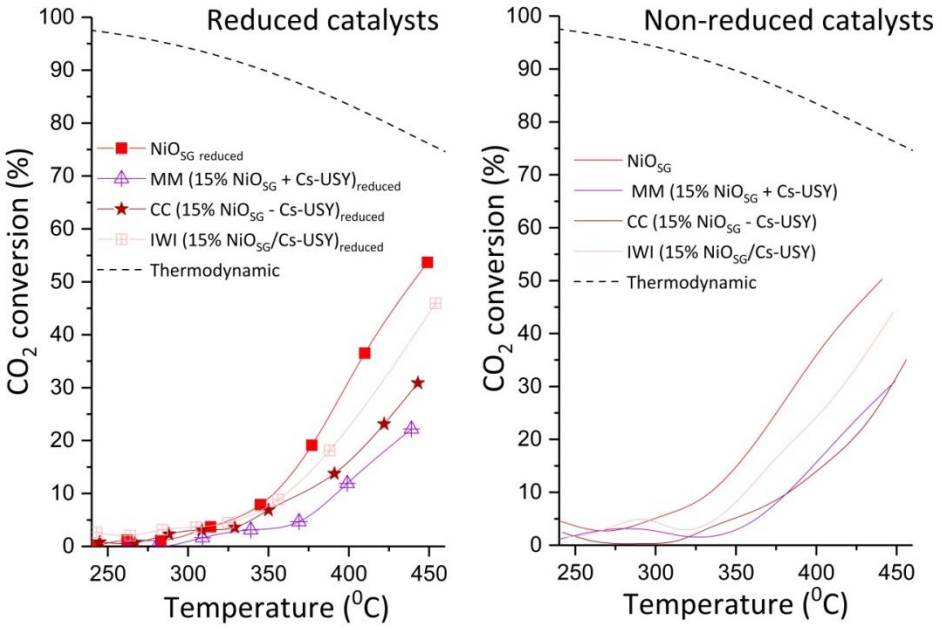

Figure 30: CO_2 conversion of sol- gel catalyst (reduced vs. non-reduced).

Regarding selectivity to methane, results follow the trend: NiO_{SG} > IWI > CC > MM. Anyway, the performances of the sol-gel materials are considerably lower than those reported for impregnated samples in previous chapters.

Table 8: Temperature vs. selectivity data for Sol-gel catalysts.

Catalysts	Temperature (^{0}C)	CH_4 Selectivity$_{non-reduced}$ (%)	CH_4 Selectivity$_{reduced}$ (%)
NiO_{SG}	240	96	-
	280	79	35
	320	66	38
	360	60	37
	400	94	51
	440	99	71
MM [15% NiO_{SG} + Cs-USY]	240	95	-
	280	86	-
	320	19	38
	360	4	9

	400	37	30
	440	82	99
CC [15% NiO_{SG} - Cs-USY]	240	-	86
	280	-	76
	320	-	58
	360	42	53
	400	42	43
	440	43	43
IWI [15% NiO_{SG}/Cs-USY]	240	97	96
	280	95	85
	320	82	61
	360	68	47
	400	53	47
	440	90	52

In order to properly compare the different samples in terms of Ni active sites per test, samples performances were depicted per gram of Ni in Figure 31, being observed that catalysts with 15 wt.% Ni interacting with a zeolite support present better methane yields than the unsupported NiO_{SG} catalyst. This confirms that the presence of a support promotes the metal-support interactions and is beneficial for the methanation activity and selectivity, in accordance with the literature [19].

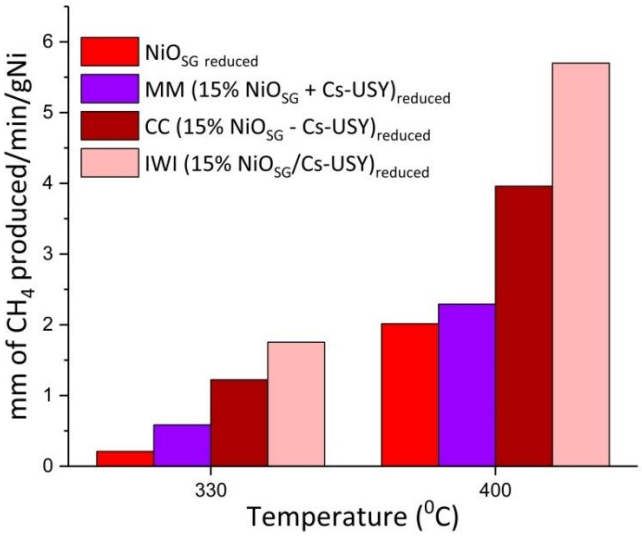

Figure 31: Methane yield of sol-gel catalyst over specific temperature (in tests with reduction treatment).

Regarding the comparison between the zeolite-containing sol-gel materials, in Figure 31 one can observe that performances follow the trend: IWI > CC > MM. These results indicate that, despite the severe structural damage induced in the zeolite by the IWI procedure, the physicochemical properties of this catalyst are the most promising towards the studied reaction. Indeed, the metal particle sizes determined for the samples after reduction (Table 7) were already indicative of the enhanced resistance towards sintering presented by this sample.

Finally, in order to easily verify the effect of the pre-reduction treatment in the samples performances, Figure 32 presents the activity of each catalyst in the tests carried out with and without reduction. One can observe that the reduction leads to a slight decrease in the performances, irrespective of the samples under analysis. This behavior can be likely due to two effects. Firstly, as already discussed in H_2 TPR results, the type of Ni species was almost the same in the catalysts before and after reduction. Consequently, the pre-reduction treatment did not lead to a significant increase in the amount of Ni^0 in the samples. Secondly, the pre-reduction treatment could lead to increases in sintering processes, which cannot be confirmed by the Scherrer equation as particle sizes are out of the equation validity range (5-50nm).

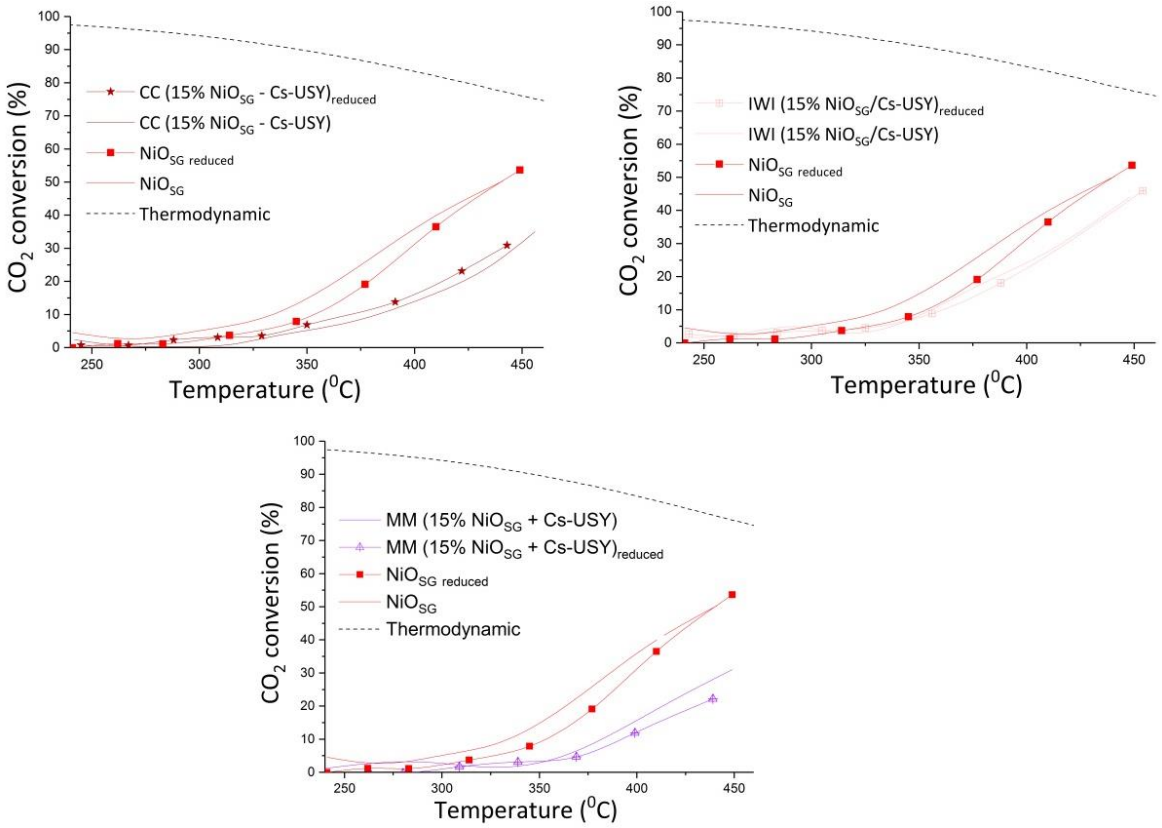

Figure 32: CO_2 conversion Vs. temperature of sol-gel catalysts.

5. Closure

5.1. Conclusion

Power-to-gas constitutes a promising technology for storing the renewable electricity surplus produced in low consumption periods into synthetic natural gas. This process starts with the production of hydrogen from water electrolysis and follows with the reduction of CO_2 into CH_4 by Sabatier reaction. CO_2 methanation is typically carried out by using heterogeneous catalysis and, among all the reported materials, Ni-based zeolites have shown potential for this reaction. However, they present limitations in terms of Ni particles average sizes, being mandatory to explore strategies for improving metallic dispersion.

In this way, in the present work, three approaches have been developed for obtaining enhanced dispersion on Ni-based CsUSY zeolites for application in CO_2 methanation. Indeed, the effects of adding different promoters (Ce, Zr, La and Y), tuning the impregnation solvent (water, ethanol, methanol, 2-propanol, acetone and ethylene glycol) and even changing of preparation method (from impregnation to sol-gel) were analyzed in terms of catalysts properties and catalytic performances.

Starting by promoters incorporation (15%Ni-15%M/Cs-USY samples), it was found that the addition of a second metal by a previously optimized impregnation method (co-impregnation) could enhance the properties of Ni species in terms of reducibility and, more important, Ni^0 average size. Among all the studied promoters, yttrium led to the highest enhancement of the catalytic performances, what could be explained by the low Ni^0 particle size, the better metal-support interactions and, probably, the favored activation of CO_2 over this sample.

Furthermore, tuning the impregnation solvent nature (15%Ni/Cs-$USY_{Solvent}$ samples) led to effects on Ni^0 particle sizes, Ni species location and structure crystallinity. However, the strength of the interaction between water and the materials was not strongly affected by the solvent used. Among all the studied solvents, 2-propanol was the one leading to the best performances both in terms of CO_2 conversion and CH_4 selectivity.

Finally, regarding the study of sol-gel as preparation method, it was found that considerably larger Ni^0/NiO particles are formed by this strategy (30-50 nm), what justifies the low activities revealed by these samples. However, it was possible to confirm that using a supported catalyst rather than the pure Ni nanoparticles is more suitable. When comparing the samples containing Cs-USY zeolite, impregnation of the Ni nanoparticles over the support was found as a better strategy than

mechanical mixture and co-calcination, even if the followed impregnation conditions could be responsible for the severe structural damage of the zeolite structure observed from XRD analysis.

5.2. Future perspectives

Taking into account the main results and conclusions resulting from the present work, future work could be suggested in order to complement the present study:

- Characterization of samples interaction with CO_2 (e.g. CO_2-TPD, CO_2 adsorption followed by Operando FTIR);
- Study of the dispersion of Ni particles over the different materials (e.g. TEM, mapping);
- Preparation of a 15%Ni-15%Y/Cs-USY zeolite using 2-propanol as solvent.

6. References

[1] D. Raynaud, B. Hingray, B. François, and J. D. Creutin, “Energy droughts from variable renewable energy sources in European climates,” *Renew. Energy*, vol. 125, pp. 578–589, 2018.

[2] W. H. J. Crijns-graus, “Global Potential of Renewable Energy Sources : a Literature Assessment,” no. 2008, 2014.

[3] B. Kirby, M. Milligan, P. Denholm, E. Ela, B. Kirby, and M. Milligan, “The Role of energy storage with renewable electricity generation,” 2010.

[4] H. Chen, T. Ngoc, W. Yang, C. Tan, and Y. Li, “Progress in electrical energy storage system : A critical review,” *Prog. Nat. Sci.*, vol. 19, no. 3, pp. 291–312, 2009.

[5] G. Centi, E. Quadrelli, and S. Perathoner, “Catalysis for CO2 conversion: a key technology for rapid introduction of renewable energy in the value chain of chemical industries,” *Energy Environ. Sci.*, vol. 6, pp. 1711–1731, 2013.

[6] S. K. Hoekman, A. Broch, C. Robbins, and R. Purcell, “CO2 recycling by reaction with renewably-generated hydrogen,” *Int. J. Greenh. Gas Control*, vol. 4, pp. 44–50, 2010.

[7] T. Schaaf, J. Grünig, M. R. Schuster, T. Rothenfluh, and A. Orth, “Methanation of CO2 - storage of renewable energy in a gas distribution system,” *Energy. Sustain. Soc.*, vol. 4, pp. 1–14, 2014.

[8] C. Mebrahtu, F. Krebs, S. Abate, S. Perathoner, G. Centi, and R. Palkovits, "CO2 Methanation: Principles and Challenges," *Horizons in Sustainable Industrial Chemistry and Catalysis*, vol. 178, pp. 85-103, 2019.

[9] J. Wu and X. D. Zhou, “Catalytic conversion of CO2 to value added fuels : Current status , challenges , and future directions,” *Chinese J. Catal.*, vol. 37, no. 7, pp. 999–1015, 2016.

[10] B. Hu, C. Guild, and S. L. Suib, “Thermal , electrochemical, and photochemical conversion of CO2 to fuels and value-added products,” *Biochem. Pharmacol.*, vol. 1, pp. 18–27, 2013.

[11] M. Younas, L. L. Kong, M. J. K. Bashir, H. Nadeem, A. Shehzad, and S. Sethupathi, “Recent Advancements , Fundamental Challenges , and Opportunities in Catalytic Methanation of CO2,” *Energy Fuels*, vol. 30, p. 8815−8831, 2016.

[12] F.-Z. Ghaib, K., Nitz, K., & Ben-Fares, “Chemical Methanation of CO2: A Review,” *ChemBioEng*

Rev., vol. 3, no. 6, pp. 266–275, 2016.

[13] M. A. A. Aziz, A. A. Jalil, S. Triwahyono, and A. Ahmad, "CO2 methanation over heterogeneous catalysts: recent progress and future prospects," *Green Chem.*, vol. 17, pp. 2647–2663, 2015.

[14] W. Wang and J. Gong, "Methanation of carbon dioxide : an overview," *Front. Chem. Sci. Eng.*, vol. 5, no. 1, pp. 2–10, 2011.

[15] J. Gao, Y. Wang, Y. Ping, D. Hu, G. Xu, and F. Su, "A thermodynamic analysis of methanation reactions of carbon oxides for the production of synthetic natural gas," *RSC Adv.*, vol. 2, pp. 2358–2368, 2012.

[16] D. J. Darensbourg and C. Ovalles, "Catalytic carbon dioxide methanation by alumina-supported mono- and polynuclear ruthenium carbonyls," *Inorg. Chem.*, vol. 25, no. 10, pp. 1603–1609, May 1986.

[17] S. Tada, O. J. Ochieng, R. Kikuchi, T. Haneda, and H. Kameyama, "Promotion of CO2 methanation activity and CH4 selectivity at low temperatures over Ru/CeO2/Al2O3 catalysts," *Int. J. Hydrogen Energy*, vol. 39, no. 19, pp. 10090–10100, 2014.

[18] A. Karelovic and P. Ruiz, "Improving the Hydrogenation Function of Pd/γ-Al2O3 Catalyst by Rh/γ-Al2O3 Addition in CO2 Methanation at Low Temperature," *ACS Catal.*, vol. 3, no. 12, pp. 2799–2812, Dec. 2013.

[19] I. Graça, L. V. González, M. C. Bacariza, A. Fernandes, C. Henriques, J. M. Lopes, and M. F. Ribeiro., "CO2 hydrogenation into CH4 on NiHNaUSY zeolites," *Appl. Catal. B Environ.*, vol. 147, pp. 101–110, 2014.

[20] C. Deleitenburg and A. Trovarelli, "Metal-Support Interactions in Rh/CeO2, Rh/TiO2, and Rh/Nb2O5 Catalysts as Inferred from CO2 Methanation Activity," *J. Catal.*, vol. 156, no. 1, pp. 171–174, 1995.

[21] A. M. Abdel-Mageed, S. Eckle, H. G. Anfang, and R. J. Behm, "Selective CO methanation in CO2-rich H2 atmospheres over a Ru/zeolite catalyst: The influence of catalyst calcination," *J. Catal.*, vol. 298, pp. 148–160, 2013.

[22] P. A. U. Aldanaa, F. Ocampo, K. Kobl, B. Louis, F. Thibault-Starzyk, M. Daturi, P. Bazin, S. Thomas, and A. C. Roger, "Catalytic CO2 valorization into CH4 on Ni-based ceria-zirconia.

Reaction mechanism by operando IR spectroscopy," *Catal. Today*, vol. 215, pp. 201–207, 2013.

[23] P. Frontera, A. Macario, M. Ferraro, and P. Antonucci, "Supported Catalysts for CO2 Methanation: A Review," *Catalysts*, vol. 7, no. 2, 2017.

[24] X. Su, J. Xu, B. Liang, H. Duan, B. Hou, and Y. Huang, "Catalytic carbon dioxide hydrogenation to methane : A review of recent studies," *J. Energy Chem.*, vol. 25, pp. 2015–2017, 2016.

[25] M. C. Bacariza, R. Bértolo, I. Graça, J. M. Lopes, and C. Henriques, "The effect of the compensating cation on the catalytic performances of Ni/USY zeolites towards CO2 methanation," *J. CO2 Util.*, vol. 21, pp. 280–291, 2017.

[26] M. C. Bacariza, I. Graça, A. Westermann, M. F. Ribeiro, J. M. Lopes, and C. Henriques, "CO2 Hydrogenation Over Ni-Based Zeolites : Effect of Catalysts Preparation and Pre-reduction Conditions on Methanation Performance," *Top. Catal.*, vol. 59, pp. 314–325, 2016.

[27] M. C. Bacariza, I. Graça, S. S. Bebiano, J. M. Lopes, and C. Henriques, "Micro- and mesoporous supports for CO2 methanation catalysts : A comparison between SBA-15 , MCM-41 and USY zeolite," *Chem. Eng. Sci.*, vol. 175, pp. 72–83, 2018.

[28] M. C. Bacariza, I. Graça, J. M. Lopes, and C. Henriques, "Tuning Zeolite Properties towards CO 2 Methanation : An Overview," *ChemCatChem,* vol. 11*,* pp. 1–14, 2019.

[29] M. C. Bacariza, I. Graça, J. M. Lopes, and C. Henriques, "Enhanced activity of CO2 hydrogenation to CH4 over Ni based zeolites through the optimization of the Si/Al ratio," *Microporous Mesoporous Mater.*, vol. 267, pp. 9–19, 2018.

[30] M. C. Bacariza, M. Maleval, I. Graça, J. M. Lopes, and C. Henriques, "Power-to-methane over Ni / zeolites : Influence of the framework type," *Microporous Mesoporous Mater.*, vol. 274, pp. 102–112, 2019.

[31] A. Westermann, B. Azambre, M. C. Bacariza, I. Graça, M. F. Ribeiro, and J. M. Lopes, "The promoting effect of Ce in the CO2 methanation performances on NiUSY zeolite : A FTIR In Situ / Operando study," *Catal. Today*, vol. 283, pp. 74–81, 2017.

[32] M. C. Bacariza, S. S. Bebiano, J. M. Lopes, and C. Henriques, "Magnesium as Promoter of CO2 Methanation on Ni-Based USY Zeolites," *Energy & Fuels*, vol. 31, no. 9, pp. 9776–9789, 2017.

[33] M. C. Bacariza, I. Graça, J. M. Lopes, and C. Henriques, “Ni-Ce/Zeolites for CO2 Hydrogenation to CH4 : Effect of the Metal Incorporation Order,” *ChemCatChem*, vol. 10, pp. 2773–2781, 2018.

[34] S. Li and J. Gong, “Strategies for improving the performance and stability of Ni-based catalysts for reforming reactions,” *Chem. Soc. Rev.*, vol. 43, pp. 7245–7256, 2014.

[35] A. Quindimil, U. De-la-torre, B. Pereda-ayo, J. A. González-marcos, and J. R. González-velasco, “Ni catalysts with La as promoter supported over Y- and BETA- zeolites for CO2 methanation,” *Appl. Catal. B Environ.*, vol. 238, no. July, pp. 393–403, 2018.

[36] A. Westermann, B. Azambre, M. C. Bacariza, I. Graça, and M. F. Ribeiro, “Insight into CO2 methanation mechanism over NiUSY zeolites : An operando IR study,” *Appl. Catal. B Environ.*, vol. 175, pp. 120–125, 2015.

[37] H. Y. Kim, H. M. Lee, and J.-N. Park, “Bifunctional Mechanism of CO2 Methanation on Pd-MgO/SiO2 Catalyst: Independent Roles of MgO and Pd on CO2 Methanation,” *J. Phys. Chem. C*, vol. 114, no. 15, pp. 7128–7131, 2010.

[38] J.-N. Park and E. W. McFarland, “A highly dispersed Pd–Mg/SiO2 catalyst active for methanation of CO2,” *J. Catal.*, vol. 266, no. 1, pp. 92–97, 2009.

[39] M. Guo and G. Lu, “The effect of impregnation strategy on structural characters and CO2 methanation properties over MgO modified Ni/SiO2 catalysts,” *Catal. Commun.*, vol. 54, pp. 55–60, 2014.

[40] J. Ren, X. Qin, J.-Z. Yang, Z.-F. Qin, H.-L. Guo, J.-Y. Lin, and Z. Li, “Methanation of carbon dioxide over Ni–M/ZrO2 (M=Fe, Co, Cu) catalysts: Effect of addition of a second metal,” *Fuel Process. Technol.*, vol. 137, pp. 204–211, 2015.

[41] P. Dumrongbunditkul, T. Witoon, M. Chareonpanich, and T. Mungcharoen, “Preparation and characterization of Co–Cu–ZrO2 nanomaterials and their catalytic activity in CO2 methanation,” *Ceram. Int.*, vol. 42, no. 8, pp. 10444–10451, 2016.

[42] A. V. Boix, M. A. Ulla, and J. O. Petunchi, “Promoting Effect of Pt on Co Mordenite upon the Reducibility and Catalytic Behavior of CO2Hydrogenation,” *J. Catal.*, vol. 162, no. 2, pp. 239–249, 1996.

[43] J. B. Branco, A. C. Ferreira, T. A. Gasche, G. Pimenta, and J. P. Leal, “Low Temperature Partial Oxidation of Methane over Bimetallic Nickel- f Block Element Oxide Nanocatalysts,” *Adv. Synth. Catal.*, vol. 356, pp. 3048–3058, 2014.

[44] A. S. Danial, M. M. Saleh, S. A. Salih, and M. I. Awad, “On the synthesis of nickel oxide nanoparticles by sol-gel technique and its electrocatalytic oxidation of glucose,” *J. Power Sources*, vol. 293, pp. 101–108, 2015.

[45] S. Aghamohammadi, M. Haghighi, and M. Maleki, “Sequential impregnation vs . sol-gel synthesized Ni/Al2O3-CeO2 nanocatalyst for dry reforming of methane : Effect of synthesis method and support promotion,” *Mol. Catal.*, vol. 431, pp. 39–48, 2017.

[46] Q. Liu and Y. Tian, “One-pot synthesis of NiO/SBA-15 monolith catalyst with a three-dimensional framework for CO 2 methanation,” *Int. J. Hydrogen Energy*, vol. 42, pp. 12295–12300, 2017.

[47] B. Lu, Y. Ju, T. Abe, and K. Kawamoto, “Grafting Ni particles onto SBA-15, and their enhanced performance for CO2 methanation,” *RSC Adv.*, vol. 5, no. 70, pp. 56444–56454, 2015.

[48] A. Trovarelli, C. Deleitenburg, G. Dolcetti, and J. L. Lorca, “CO2 Methanation Under Transient and Steady-State Conditions over Rh/CeO2 and CeO2-Promoted Rh/SiO2: The Role of Surface and Bulk Ceria,” *J. Catal.*, vol. 151, no. 1, pp. 111–124, 1995.

[49] S. Rahmani, M. Rezaei, and F. Meshkani, “Preparation of promoted nickel catalysts supported on mesoporous nanocrystalline gamma alumina for carbon dioxide methanation reaction,” *J. Ind. Eng. Chem.*, vol. 20, no. 6, pp. 4176–4182, 2014.

[50] W. Ahmad, M. N. Younis, R. Shawabkeh, and S. Ahmed, “Synthesis of lanthanide series (La, Ce, Pr, Eu & Gd) promoted Ni/γ-Al2O3 catalysts for methanation of CO2 at low temperature under atmospheric pressure,” *Catal. Commun.*, vol. 100, pp. 121–126, 2017.

[51] Y. Shu, L. E. Murillo, J. P. Bosco, W. Huang, A. I. Frenkel, and J. G. Chen, “The effect of impregnation sequence on the hydrogenation activity and selectivity of supported Pt/Ni bimetallic catalysts,” *Appl. Catal. A Gen.*, vol. 339, no. 2, pp. 169–179, 2008.

[52] J. R. A. Sietsma, J. D. Meeldijk, M. V. -Helder, A. Broersma, A. J. Dillen, P. E. Jongh, and K. P. Jong, “Ordered Mesoporous Silica to Study the Preparation of Ni/SiO2 ex Nitrate Catalysts:

Impregnation, Drying, and Thermal Treatments," *Chem. Mater.*, vol. 20, no. 9, pp. 2921–2931, 2008.

[53] S. Qiu, Q. Zhang, W. Lv, T. Wang, Q. Zhang, and L. Ma, "Simply packaging Ni nanoparticles inside SBA-15 channels by co-impregnation for dry reforming of methane," *RSC Adv.*, vol. 7, pp. 24551–24560, 2017.

[54] W. Trisunaryanti, E. Suarsih, and I. I. Falah, "Well-dispersed nickel nanoparticles on the external and internal surfaces of SBA-15 for hydrocracking of pyrolyzed α-cellulose," *RSC Adv.*, vol. 9, pp. 1230–1237, 2019.

[55] A. F. Lucredio, J. D. A. Bellido, A. Zawadzki, and E. M. Assaf, "Co catalysts supported on SiO2 and Gamma-Al2O3 applied to ethanol steam reforming : Effect of the solvent used in the catalyst preparation method," *Fuel*, vol. 90, no. 4, pp. 1424–1430, 2011.

[56] Y. Zhang, Y. Liu, G. Yang, Y. Endo, and N. Tsubaki, "The solvent effects during preparation of Fischer – Tropsch synthesis catalysts : Improvement of reducibility , dispersion of supported cobalt and stability of catalyst," *Catal. Today*, vol. 142, pp. 85–89, 2009.

[57] S.-W. Ho and Y.-S. Su, "Effects of Ethanol Impregnation on the Properties of Silica-Supported Cobalt Catalysts," *J. Catal.*, vol. 168, no. 1, pp. 51–59, 1997.

[58] H. Song and U. Ozkan, "The role of impregnation medium on the activity of ceria-supported cobalt catalysts for ethanol steam reforming," *J. Mol. Catal. A Chem.*, vol. 318, pp. 21–29, 2010.

[59] U. Rodemerck, M. Schneider, and D. Linke, "Improved stability of Ni/SiO2 catalysts in CO2 and steam reforming of methane by preparation via a polymer-assisted route," *Catal. Commun.*, vol. 102, pp. 98–102, 2017.

[60] S. Ali, M. J. Almarri, A. G. Abdelmoneim, A. Kumar, and M. M. Khader, "Catalytic evaluation of nickel nanoparticles in methane steam reforming," *Int. J. Hydrogen Energy*, vol. 41, pp. 1–10, 2016.

[61] A. E. Danks, S. R. Hall, and Z. Schnepp, "The evolution of 'sol–gel' chemistry as a technique for materials synthesis," *Mater. Horizons*, vol. 3, pp. 91–112, 2016.

[62] M. Che and J. C. Ve, *Characterization of Solid Materials and Heterogeneous Catalysts: From*

Structure to Surface Reactivity. John Wiley & Sons, 2012.

[63] H. G. Karge and J. Weitkamp, *Characterization II*. Springer, 2007.

[64] A. Jentys and J. A. Lercher, "Techniques of zeolite characterization," *Surf. Sci. Catal.*, vol. 137, pp. 345–386, 2001.

[65] F. Pinna, "Supported metal catalysts preparation," *Catal. Today*, vol. 41, pp. 129–137, 1998.

[66] R. Alotaibi, F. Alenazey, F. Alotaibi, and N. Wei, "Ni catalysts with different promoters supported on zeolite for dry reforming of methane," *Appl. Petrochemical Res.*, vol. 5, no. 4, pp. 329–337, 2015.

[67] A. Quindimil, U. De-La-Torre, B. Pereda-Ayo, J. A. González-Marcos, and J. R. González-Velasco, "Ni catalysts with La as promoter supported over Y- and BETA- zeolites for CO2 methanation," *Appl. Catal. B Environ.*, vol. 238, pp. 393–403, 2018.

[68] M. A. Goula, G. I. Siakavelas, K. N. Papageridis, and N. D. Charisiou, "Hydrogen production via the glycerol steam reforming reaction over Ni/ZrO2 and Ni/SiO2-ZrO2 catalysts," in *Conference: 21st World Hydrogen Energy Conference (WHEC2016), At Zaragoza, Spain*, 2016.

[69] G. Y. Ramírez-Hernández, T. Viveros-García, R. Fuentes-Ramírez, and I. R. Galindo-Esquivel, "Promoting behavior of yttrium over nickel supported on alumina-yttria catalysts in the ethanol steam reforming reaction," *Int. J. Hydrogen Energy*, vol. 41, no. 22, pp. 9332–9343, 2016.

[70] H. Takano, Y. Kirihata, K. Izumiya, N. Kumagai, H. Habazaki, and K. Hashimoto, "Highly active Ni/Y-doped ZrO2 catalysts for CO2 methanation," *Appl. Surf. Sci.*, vol. 388, pp. 653–663, 2016.

[71] M. Jafari, A. Nouri, M. Kazemimoghadam, and T. Mohammadi, "Investigations on hydrothermal synthesis parameters in preparation of nanoparticles of LTA zeolite with the aid of TMAOH," *Powder Technol.*, vol. 237, pp. 442–449, 2013.

Annexes

I. Detailed procedure for determining the catalytic performances

During the catalytic experiences and according to the figure presented below, several data were recorded: temperature ($T_{reaction}$), [CO_2], [CO] and [CH_4] in volume % and Q_{outlet}.

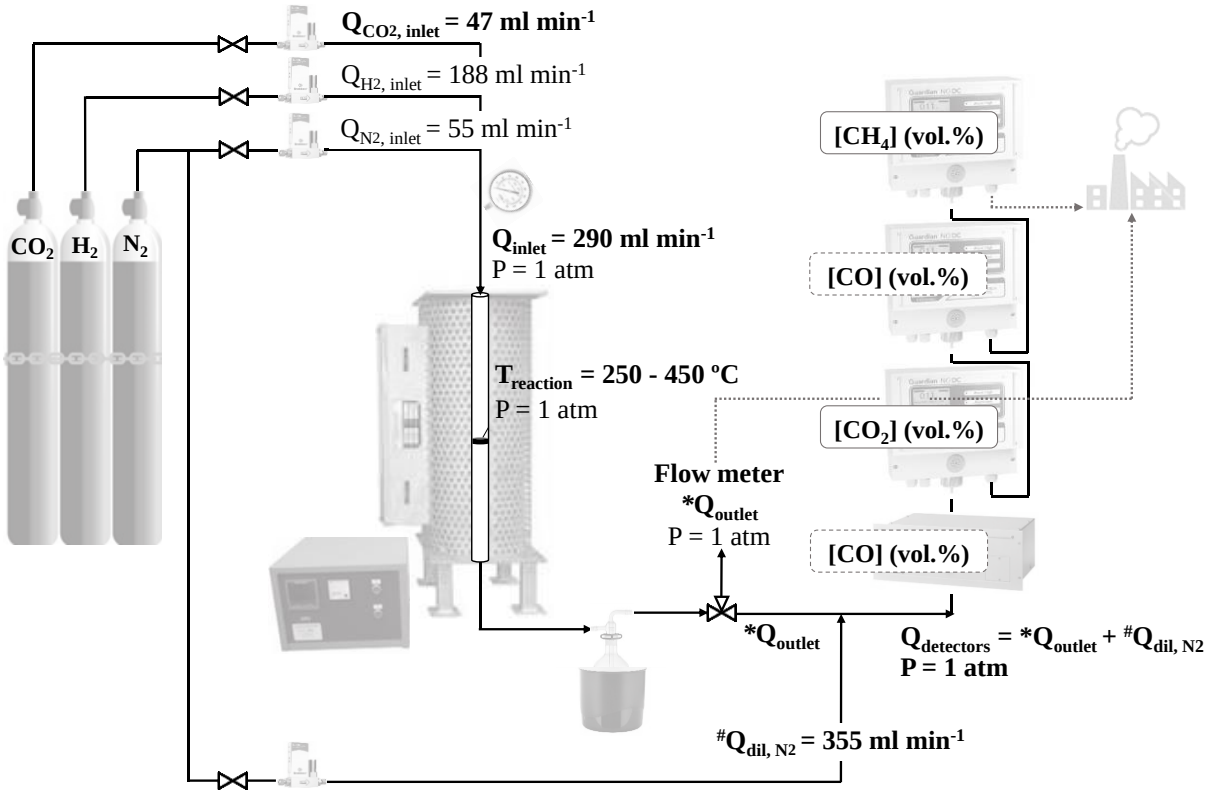

All the flows were measured at the same conditions (T, P) using the flow meter present in one of the lines coming from the 3-ways valve. Indeed, the inlet volumetric flows of the reactants in absence of reaction (total flow of 290 ml min^{-1} with 188, 47 and 55 ml min^{-1} of H_2, CO_2 and N_2, respectively), were measured passing the gases through the reactor without catalyst, heating at the same reaction temperatures studied in the tests and, finally, passing through the water trap before reaching the flow meter(Q_{inlet}). Thus, it was guaranteed that the conditions (P, T) used for the measurement of the outlet flows with and without reaction were the same. Additionally, under reaction conditions and with a catalyst in the reactor bed, the outlet flows in dry base (Q_{outlet}) and the reactants concentrations ([CO_2], [CO] and [CH_4]) were measured in the flow meter and in the detectors, respectively, after passing through the water trap. As a result, and according to the ideal gases equation, it will be equivalent to use volumetric or molar flows for the determination of the catalytic

performances. Additionally, the incorporation of a fixed flow of inert ($Q_{dil,\,N_2}$ = 355 ml min^{-1}) in the stream going to the detectors has to be taken into account. The calculation of the conversion and selectivity for a certain $T_{reaction}$ was done in three steps:

a. **Determination of the $Q_{detectors}$:**

$$Q_{detectors}\,(ml/min) = Q_{outlet} + Q_{dil,\,N_2} = Q_{outlet} + 355$$

b. **Conversion of the [CO_2], [CO] and [CH_4] (vol.%) into $Q_{CO2,outlet}$, $Q_{CO,outlet}$, $Q_{CH4,outlet}$ (as the dilution stream contains only N_2, the flow of the reactants in the detectors flow will be the same than in the outlet flow in dry base (after removing water)):**

$$Q_{CO_2,outlet}(ml\ min^{-1}) = Q_{CO_2,detectors} = [CO_2] \cdot Q_{detectors}$$

$$Q_{CO,outlet}\,(ml\ min^{-1}) = Q_{CO,detectors} = [CO] \cdot Q_{detectors}$$

$$Q_{CH_4,outlet}(ml\ min^{-1}) = Q_{CH_4,detectors} = [CH_4] \cdot Q_{detectors}$$

c. **Calculation of the conversion and selectivity with the volumetric flows (as the P, T conditions of the measurements were the same):**

$$CO_2\ conversion\ (\%) = \frac{Q_{CO_2,inlet} - Q_{CO_2,outlet}}{Q_{CO_2,inlet}} \cdot 100$$

$$CH_4\ selectivity\ (\%) = \frac{Q_{CH_4,outlet}}{Q_{CO_2,inlet} - Q_{CO_2,outlet}} \cdot 100$$

$$CO\ selectivity\ (\%) = \frac{Q_{CO,outlet}}{Q_{CO_2,inlet} - Q_{CO_2,outlet}} \cdot 100$$